Differential requirement of MED14 and UVH6 for heterochromatin transcription upon destabilization of silencing

Pierre Bourguet[1], Stève de Bossoreille[1,2†], Leticia López-González[1†], Marie-Noëlle Pouch-Pélissier[1], Ángeles Gómez-Zambrano[1,3], Anthony Devert[1], Thierry Pélissier[1], Romain Pogorelcnik[1], Isabelle Vaillant[1], Olivier Mathieu[1*]

[1] Université Clermont Auvergne, CNRS, Inserm, Génétique Reproduction et Développement (GReD), F-63000 Clermont-Ferrand, France

[2] Present address: Laboratoire Reproduction et Développement des Plantes, Université de Lyon, ENS de Lyon, UCB Lyon 1, CNRS, INRA, F-69342, Lyon, France

[3] Present address: Instituto de Bioquímica Vegetal y Fotosíntesis, CSIC-Cartuja, Avda. Américo Vespucio, 49. 41092-Sevilla- Spain

† These authors contributed equally to this work

* Corresponding author. Tel: 33 473 407 407, E-mail: olivier.mathieu@uca.fr

Abstract

Constitutive heterochromatin is commonly associated with high levels of repressive epigenetic marks and is stably maintained transcriptionally silent by the concerted action of different, yet convergent, silencing pathways. Reactivation of heterochromatin transcription is generally associated with alterations in levels of these epigenetic marks. However, in mutants for particular epigenetic regulators, or upon particular environmental changes such as heat stress, heterochromatin-associated silencing is destabilized without noticeable changes in epigenetic marks. This suggests that transcription can occur in a non-permissive chromatin context, yet the factors involved remain poorly known. Here, we show that heat stress-induced transcription of heterochromatin depends on the TFIIH component UVH6 and the Mediator subunit MED14. Mutants for these two factors exhibit hypersensitivity to heat stress, and under these conditions, UVH6 and MED14 are required for transcription of a high number of loci. We further show that MED14, but not UVH6, is required for transcription when heterochromatin silencing is destabilized in the absence of stress. In this case, MED14 requires proper chromatin patterns of repressive epigenetic marks for its function. We also uncover that MED14 regulates non-CG DNA methylation at a subset of RNA-directed DNA methylation target loci. These findings provide insight into the control of heterochromatin transcription upon silencing destabilization and identify MED14 as a regulator of DNA methylation.

Introduction

In eukaryotic cells, DNA associates with proteins to form chromatin, which is organized in two main states, namely euchromatin and heterochromatin. Compared with the gene-rich euchromatin, heterochromatin is a highly compacted organization of chromatin and mostly comprises different types of repeated sequences, notably transposable elements (TEs). Heterochromatin generally associates with high levels of cytosine DNA methylation and specific histone post-translational modifications, which in *Arabidopsis thaliana* are dimethylation at histone H3 lysine 9 (H3K9me2) or monomethylation of H3K27 (H3K27me1) (Feng and Michaels, 2015). These epigenetic marks typically contribute to maintaining heterochromatin compacted and transcriptionally inactive. In Arabidopsis, H3K27me1 is catalyzed by the histone methyltransferases ARABIDOPSIS TRITHORAX-RELATED PROTEIN 5 (ATXR5) and ATXR6 (Jacob et al., 2009). H3K9me2 is deposited by the histone methyltransferases KRYPTONITE (KYP)/SU(VAR)3–9 HOMOLOG 4 (SUVH4), SUVH5, and SUVH6. In plants, cytosine DNA methylation occurs in three sequence contexts: CG, CHG and CHH, where H is any base but a guanine. CG methylation is maintained during DNA replication, where METHYLTRANSFERASE 1 (MET1) reproduces the CG methylation pattern from the template strand to the neo-synthetized strand (Law and Jacobsen, 2010). CHG methylation is predominantly mediated by CHROMOMETHYLTRANSFERASE 3 (CMT3), which is recruited to its target sites by binding to H3K9me2 (Du et al., 2012). CHH methylation depends on the activity of both CMT2 and a complex pathway termed RNA-directed DNA Methylation (RdDM), which is notably operated by the plant specific RNA polymerases IV (Pol IV) and V (Pol V) (Law and Jacobsen, 2010; Stroud et al., 2014; Zemach et al., 2013). RdDM relies on small siRNA precursors generated by Pol IV, maturated by RNA DEPENDENT RNA POLYMERASE 2 (RDR2) and processed by DICER-LIKE 3 (DCL3) in 24-nucleotide siRNAs that are loaded into ARGONAUTE 4 (AGO4) (Matzke and Mosher, 2014). In the canonical model, base pairing of Pol V-dependent scaffold transcripts with AGO4-bound siRNAs recruits DOMAINS REARRANGED METHYLTRANSFERASE 2 (DRM2) to its target sites (Wendte and Pikaard, 2017). Chromatin remodelers also participate in DNA methylation, with DEFECTIVE IN RNA-DIRECTED DNA METHYLATION 1 (DRD1) promoting CHH methylation at RdDM-dependent loci, while DECREASE IN DNA METHYLATION 1 (DDM1) would allow all methyltransferases to access heterochromatin thereby contributing to DNA methylation in all sequence contexts (Kanno et al., 2004; Stroud et al., 2013; Vongs et al., 1993; Zemach et al., 2013).

Although a certain level of transcription of some heterochromatin sequences is required for establishing or maintaining heterochromatin structure, DNA methylation and histone modifications contribute different layers of silencing that largely repress heterochromatin transcription. Additional factors appear to ensure transcriptional silencing at subsets of heterochromatin loci largely independently of these marks. The best described are MORPHEUS' MOLECULE 1 (MOM1), REPLICATION PROTEIN A2 (RPA2), BRUSHY1 (BRU1), proteins of the Arabidopsis MICRORCHIDIA family (AtMORC), and the MAINTENANCE OF MERISTEMS (MAIN) and MAIN-LIKE 1 (MAIL1) proteins that likely act in complex (Amedeo et al., 2000; Elmayan et al., 2005; Han et al., 2016; Ikeda et al., 2017; Kapoor et al., 2005; Moissiard et al., 2012, 2014; Takeda et al., 2004). Although little is known about the mode of action of these proteins, MAIL1/MAIN and AtMORC6 appear to contribute to heterochromatin compaction, while MOM1 does not in spite of its heterochromatic localization (Feng et al., 2014; Ikeda et al., 2017; Probst et al., 2003; Wang et al., 2015).

Some environmental challenges such as heat stress can also transiently alleviate heterochromatin silencing without disturbing epigenetic marks (Lang-Mladek et al., 2010; Pecinka et al., 2010; Tittel-Elmer et al., 2010). Importantly, heat-induced release of silencing does not occur through inhibition of known silencing pathways

nor does it depend on the master regulator of the heat stress transcriptional response HsfA2 (Pecinka et al., 2010; Tittel-Elmer et al., 2010). The H2A.Z histone variant is involved in ambient temperature sensing (Kumar and Wigge, 2010), but its role in heat-induced heterochromatin transcription is unknown. Recent reports suggest that DDM1 and MOM1 act redundantly to re-establish silencing after heat stress, while heat-induced expression of the silenced gene *SDC* participates in heat stress tolerance (Iwasaki and Paszkowski, 2014; Sanchez and Paszkowski, 2014). Interestingly, HIT4 is localized at heterochromatin and is required for its transcription in heat stress but not in the *mom1* mutant (Wang et al., 2013, 2015).

Heterochromatin transcription has been observed in a variety of model organisms under various conditions (Castel and Martienssen, 2013; Chan and Wong, 2012; Negi et al., 2016; Saksouk et al., 2015; Valgardsdottir et al., 2008). Despite its prevalence, heterochromatin transcription is a rather poorly understood process. Notably, how the transcriptional machinery can access to a repressive chromatin environment remains a largely unsolved question (Feng and Michaels, 2015). To gain insight into this mechanism, we used forwards genetics with a reporter-based system and identified the evolutionary conserved factors XPD/UVH6 and MED14 as required for heterochromatin transcription during heat stress in *Arabidopsis thaliana*. When heterochromatin silencing is destabilized by mutations in silencing factors, UVH6 is dispensable for transcription, while MED14 participates in transcription specifically if proper patterns of repressive epigenetic marks are preserved. MED14 also targets highly methylated TEs under normal growth conditions, suggesting a role for the repressive chromatin environment in recruiting MED14. We further show that MED14 regulates non-CG methylation at a subset of loci, likely through RdDM, indicating that MED14 is simultaneously involved in the transcription and the formation of heterochromatin.

Results

AtMORC6 and H2A.Z are not involved in release of silencing triggered by heat stress

We and others previously demonstrated that destabilization of silencing by heat stress does not rely on compromising DNA methylation maintenance, RNA-directed DNA methylation, histone deacetylation, HsfA2 or MOM1 functions (Lang-Mladek et al., 2010; Pecinka et al., 2010; Tittel-Elmer et al., 2010). We assessed the possible involvement of AtMORC6 and H2A.Z in this process by submitting *atmorc6-3* and *arp6-1* mutants to our previously published heat-stress conditions (Tittel-Elmer et al., 2010). AtMORC6 is required for transcriptional silencing of several repeats and TEs mostly independently of DNA methylation (Moissiard et al., 2012). ARP6 is involved in assembling H2A.Z-containing nucleosomes, which were shown to be essential to perceiving ambient temperature (Kumar and Wigge, 2010). Reverse transcription followed by quantitative PCR (RT-qPCR) assays at five selected TEs showed transcript over-accumulation under heat stress in WT plants and this over-accumulation was not significantly affected in *atmorc6-3* and *arp6-1* mutant backgrounds (supplementary figure 1). This suggests that AtMORC6 and deposition of H2A.Z are not necessary for destabilization of silencing induced by heat stress.

Heat stress-induced release of heterochromatin transcriptional silencing is independent of genome-wide changes in DNA methylation patterns

The Arabidopsis L5 transgenic line contains tandem-repetitions of a transcriptionally silent ß-glucuronidase (*GUS*) transgene under control of the cauliflower mosaic virus 35S promoter (Elmayan et al., 2005; Morel et al., 2000). Exposing L5 plants to various heat stress regimes leads to transcriptional de-repression of the *L5*-

GUS transgene as well as numerous endogenous heterochromatin loci (Lang-Mladek et al., 2010; Pecinka et al., 2010; Tittel-Elmer et al., 2010).

We sought to identify genes required for heat stress-induced activation of heterochromatin transcription using a forward genetics approach, by screening a mutagenized L5 population for reduced *L5-GUS* expression following heat stress treatment. Because such mutants may potentially be hypersensitive to heat stress and because plants do not survive histochemical detection of GUS accumulation, we set up a screening strategy that consisted in performing GUS staining on isolated leaves from 2-week-old seedlings after incubation at either 23°C or 37°C for 24h (figure 1A). Similar to whole seedlings submitted to a 4°C / 37°C temperature shift (Tittel-Elmer et al., 2010), incubating isolated leaves at 37°C led to a robust silencing release of the *L5-GUS* transgene and endogenous repeats and TEs (figure 1A, B, C). To further validate the screening method, we defined the impact of this heat stress on gene expression genome-wide, comparing transcriptomes generated by mRNA sequencing (mRNA-seq) in leaves of L5 seedlings (hereafter referred as to WT) following incubation at either 23°C or 37°C. Consistent with previous results from ATH1 microarray analysis of whole seedlings exposed to a 4°C-37°C temperature shift (Tittel-Elmer et al., 2010), we found that regions of constitutive heterochromatin, including centromeric, pericentromeric DNA and the heterochromatin knob on chromosome 4, were overall transcriptionally activated following incubation at 37°C (figure 1D). Our mRNA-seq analysis identified a total of 116 up-regulated TEs, mostly located in pericentromeric heterochromatin, confirming that these stress conditions alleviate heterochromatin-associated silencing (figure 1D). *ONSEN* elements represented notable exceptions amongst TEs in that they are predominantly located on chromosome arms yet they are highly activated by heat stress (figure 1D). This is consistent with previous observations in seedlings exposed to heat stress (Ito et al., 2011; Pecinka et al., 2010; Tittel-Elmer et al., 2010), and occurs owing to the presence of heat-responsive elements in *ONSEN* LTRs (Cavrak et al., 2014). Conversely, transcripts originating from loci located on chromosome arms tended to be downregulated after 37°C treatment (figure 1D). Accordingly, protein-coding genes (PCGs) with downregulated transcript levels were more abundant than upregulated ones (4308 vs. 1487, respectively), a tendency we also previously reported when applying stress on seedlings (Tittel-Elmer et al., 2010). Therefore, applying heat stress to isolated leaves largely mimics the transcriptional response occurring in stressed whole seedlings.

Previous analyses of DNA methylation levels at selected heterochromatin repeats and TEs using methylation-sensitive restriction enzymes have suggested that heat stress-induced alleviation of silencing does not correlate with changes in DNA methylation (Pecinka et al., 2010; Tittel-Elmer et al., 2010). To determine with high resolution whether our heat stress procedure impacts DNA methylation, we profiled cytosine methylation patterns in WT leaves at 23°C and 37°C by whole-genome bisulfite sequencing (BS-seq). Comparison of methylation levels along chromosomes and along all PCGs and TEs revealed no overall impact of heat stress exposure on DNA methylation (figure 1E and supplementary figure 2A). Furthermore, TEs and PCGs transcriptionally upregulated by heat stress displayed similar DNA methylation profiles at 23°C and 37°C (figure 1F). Notably, PCGs upregulated by heat stress showed higher average WT DNA methylation levels at CG sites than downregulated PCGs (supplementary figure 2B). Together, these results indicate that heat stress-induced transcriptional changes occur largely independently of detectable variation in DNA methylation patterns.

Mutants for *UVH6* and *MED14* are deficient for heat stress-induced release of silencing

From the ethyl methanesulfonate (EMS)-mutagenized L5 population, we isolated two mutants that we named *zen1* and *zen2,* which leaves showed reduced GUS staining following incubation at 37°C compared to stressed leaves of the non-mutagenized progenitor L5 line (figure 2A). RT-qPCR analyses indicated that decreased GUS staining was associated with reduced transcriptional activation of the *L5-GUS* transgene (figure 2B). Likewise, transcript accumulation from the heterochromatic endogenous loci *TSI*, *106B* and *MULE* was drastically reduced following heat stress in *zen1* and *zen2* compared to the WT (figure 2C), demonstrating that suppression of heat stress-mediated release of TGS in *zen1* and *zen2* is not restricted to the *L5* transgene.

The reduced silencing release in stressed *zen* mutants followed a 1:3 (mutant:WT) segregation ratio in F2 populations of *zen1* x L5 and *zen2* x L5 backcrosses, indicating that *zen1* and *zen2* are single, nuclear, recessive mutations. F1 plants from complementation tests between *zen* mutants showed a WT-like response to heat stress, demonstrating that *zen1* and *zen2* mutations affect distinct genes (supplementary figure 3A). Under normal growth conditions, *zen1* plants showed reduced leaf size, altered color and late flowering, whereas *zen2* seedlings displayed no obvious developmental phenotype (figure 2D). Survival assays revealed that both mutants were hypersensitive to heat stress relative to the WT (figure 2E). We identified candidate mutations in *zen1* and *zen2* using mapping-by-sequencing from outcross F2 populations (supplementary figure 3B, C). *zen1* plants contained a G to A transition in the *MED14* (AT3G04740) gene, changing tryptophan for a stop codon at amino acid position 1090 (figure 2G). We identified a C to T mutation in the *UVH6* (AT1G03190) gene in *zen2* plants, causing a proline to leucine substitution at amino acid 320 (figure 2G). Complementation of *zen1* and *zen2* phenotypes with transgenes encoding WT versions of MED14 and UVH6 confirmed that *MED14* and *UVH6* mutations were responsible for the phenotypes observed in *zen1* and *zen2*, respectively (figure 2F). Hence, *zen1* and *zen2* were renamed *med14-3* and *uvh6-3,* respectively.

MED14 is the central subunit of the MEDIATOR complex, a large protein complex required for early steps of transcription initiation (Cevher et al., 2014; Soutourina, 2018). In Arabidopsis, MED14 function has been involved in cell proliferation and expression regulation of some cold-regulated or biotic stress-induced genes (Autran et al., 2002; Gonzalez et al., 2007; Hemsley et al., 2014; Wang et al., 2016; Zhang et al., 2013). UVH6 is the Arabidopsis ortholog of the human XPD and yeast RAD3 proteins (Liu et al., 2003), which are part of the transcription factor IIH (TFIIH) complex involved in transcription initiation and nucleotide excision repair (Compe and Egly, 2012). XPD is an ATP-dependent 5'->3' helicase and all amino acids required for XPD functions in yeast and human show remarkable conservation in UVH6 (Kunz et al., 2005). Interestingly, all the mutations identified in *UVH6* disrupt conserved residues (supplementary figure 4). In Arabidopsis, the UVH6 function was first described as necessary for tolerance to UV damage and heat stress (Jenkins et al., 1995, 1997). Failure to isolate homozygous mutants for *uvh6-2*, a transfer-DNA (T-DNA) insertion line, suggested *UVH6* to be an essential gene (Liu et al., 2003). Supporting this conclusion, we also failed to obtain homozygous plants for another *uvh6* T-DNA insertion line (*uvh6-5*) (figure 2G).

Transcriptomic analysis of *uhv6* and *med14* mutants in the absence of stress

To investigate the impact of *med14-3* and *uvh6-3* mutations on transcription genome-wide, we determined mRNA profiles of mutant leaves following incubation at either 23°C (*med14-3*_23, *uvh6-3*_23) or 37°C (*med14-3*_37, *uvh6-3*_37) by mRNA-seq. In this analysis, we also profiled the transcriptome at 23°C of another mutant allele of *UVH6* (*uvh6-4*), which we isolated later while pursuing screening our L5 mutant

population (supplementary figure 5A, B). The *uvh6-4* mutation replaces a proline for a leucine at amino acid position 532 (figure 2G). Unlike *uvh6-3*, *uvh6-4* mutants showed yellow-green leaves and reduced stature, a phenotype similar to the one previously described for the *uvh6-1* mutant (supplementary figure 5C) (Jenkins et al., 1997). Suppression of heat stress-induced release of silencing was stronger in *uvh6-4* than in *uvh6-3* (supplementary figure 5B), and survival assays showed that *uvh6-4* and *uvh6-1* plants were more sensitive to heat stress than *uvh6-3* plants (figure 2E). This indicates that *uvh6-4* is a stronger mutant allele of *UVH6* than *uvh6-3.*

We first compared the mutant transcriptomes with that of the WT in the absence of heat stress. By applying stringent thresholds (fold change ≥ 4, false discovery rate < 0.01), we identified 628 differentially expressed genes (DEGs) in *med14-3*_23 (figure 3A), predominantly PCGs (597). As expected for a mutation of a protein required for transcription, the majority of *med14-3* DEGs (385), including 23 TEs, showed decreased transcript accumulation. Only 7 DEGs were detected in *uvh6-3*_23, while 218 loci show differential transcript accumulation in *uvh6-4*_23, in agreement with *uvh6-4* being a stronger mutant allele of *UVH6*. Unexpectedly, out of the 218 *uvh6-4*_23 DEGs, 156 were upregulated, suggesting that UVH6 mainly represses transcription at a subset of genomic loci at 23°C (figure 3A). Loci downregulated in *uvh6-4* (62) also show reduced transcript accumulation in *uvh6-3* (supplementary figure 6A). The *med14* and *uvh6* mutations affect transcript accumulation at largely independent sets of loci (figure 3B).

Gene ontology analysis indicated that genes upregulated in *med14-3*_23 were enriched for biotic stress response genes (supplementary table 1). A similar enrichment was observed in *uvh6-4*_23 upregulated genes and in genes commonly upregulated in *med14-3*_23 and *uvh6-4*_23, indicating that MED14 and UVH6 repress genes involved in pathogen response. PCGs downregulated in *med14-3*_23 were enriched for genes associated with “positive regulation of transcription from RNA polymerase II promoter in response to heat stress”. These included *HsfB2A*, *HsfA4A*, *HsfA6b* and *HsfA3*. *HsfA6b, HsfA3* and another *med14-3*_23 downregulated gene, *DREB2A*, are partially required for thermotolerance (Huang et al., 2016; Sakuma et al., 2006; Schramm et al., 2007), suggesting that downregulation of these genes might be responsible for *med14-3* hypersensitivity to heat stress (figure 2E). PCGs downregulated in *uvh6-4*_23 were enriched for genes associated with “response to UV” as well as genes involved in processes such as “anthocyanin biosynthesis”, “regulation of flavonoids”, “phenylpropanoid metabolism”, which protect plants against UV radiation (Jansen et al., 1998). Therefore, downregulation of these genes likely plays a role in *uvh6* mutant UV hypersensitivity (supplementary figure 6B) (Jenkins et al., 1995).

Genome-wide suppression of heat-stress-induced transcriptional activation in *uvh6* and *med14*

To assess the impact of *med14* and *uvh6* on transcript levels following heat stress, we compared *med14-3*_37 and *uvh6-3*_37 with WT-37 mRNA-seq datasets. Overall, heat stress-induced transcriptional activation of pericentromeric sequences was diminished in *med14* and *uvh6* mutant backgrounds, and transcripts from loci located on chromosome arms tended to accumulate at a lower level than in stressed WT plants (figure 4A). Compared with *med14*, the impact of the *uvh6* mutation on stress-induced transcriptional changes appeared more global (figure 4A, supplementary figure 7). Accordingly, the number of DEGs was higher in *uvh6-3*_37 than in *med14-3*_37. We defined 1631 DEGs in *med14-3*_37, with the vast majority (1239) showing downregulation (figure 4B). Downregulated loci included 1124 PCGs and 115 TEs. While we detected only 7 DEGs in *uvh6-3*_23 (figure 3A), more than 6200 loci were differentially expressed in *uvh6-3*_37, with 80% of these (4949) being downregulated. A total of 4711 PCGs and 238 TEs displayed less

transcript accumulation in *uvh6-3*_37 relative to WT-37 (figure 4B). The higher number of DEGs at 37°C relative to 23°C in the mutants indicates that MED14 and UVH6 functions are required for efficient transcription of a higher number of loci under heat stress.

PCGs upregulated by heat stress showed overall reduced transcript levels in *uvh6-3* and *med14-3*, while transcript accumulation of PCGs downregulated by heat stress showed limited changes in *med14-3* compared with *uvh6-3* (supplementary figure 8A, B), suggesting again a more global impact of the *uvh6* mutation on stress-induced transcriptional changes.

In the absence of stress, the *med14* and *uvh6* mutations affect transcript accumulation at rather few, largely independent set of loci (figure 3B). Under heat stress, many loci downregulated in *med14-3* were similarly affected in *uvh6-3* (figure 4C). Even though this could be expected given the large number of genes downregulated in *uvh6-3,* we also observed that loci upregulated in one mutant also showed a similar tendency in the other (figure 4C, supplementary figure 8C). This is remarkable as in both mutants, upregulation events are rare relative to downregulation events. These data suggest that MED14 and UVH6 have converging functions at many overlapping loci under heat-stress conditions.

TEs transcriptionally upregulated by heat stress showed overall reduced transcriptional activation in the mutant backgrounds (figure 4D). Heat stress predominantly destabilized silencing at TEs of the DNA/En-Spm, DNA/MuDR, LTR/Copia and LTR/Gypsy superfamilies (supplementary figure 8D). Among these stress-induced TEs, TEs downregulated in *uvh6-3*_37 showed comparable proportions. Noticeably, TEs downregulated in *med14-3*_37 were enriched in LTR/Copia and LTR/Gypsy elements, suggesting that MED14 is preferentially required for heat-induced release of silencing at LTR retrotransposons.

We generated *med14-3 uvh6-3* double mutants and assessed transcript accumulation from *L5-GUS* and selected TEs using RT-qPCR (supplementary figure 9). We found no synergy between the two mutations; at a given locus, the transcript levels in *med14-3 uvh6-3* were similar to the ones detected in the mutant showing the strongest downregulation. These results suggest that, at least at these TEs, MED14 and UVH6 function in the same molecular pathway to promote transcription.

Together, our results indicate that MED14 and UVH6 are required for proper heat stress-induced transcriptional activation of heterochromatic TEs, and more generally play an important role in controlling transcription at a high number of genomic loci under stress conditions.

Transcription of methylated TEs requires MED14 but not UVH6

Given that UVH6 and MED14 are involved in transcriptional activation induced by heat-stress, we questioned whether their functions are also required for heterochromatin transcription occurring in mutants for epigenetic regulators. To address this question, we introduced *uvh6-4* and *med14-3* in the *mom1-2* and *ddm1-2* mutant backgrounds, which display constitutive release of transcriptional silencing at heterochromatic loci, and performed mRNA-seq. In *ddm1,* loss of silencing is associated with a strong reduction in DNA, H3K9me2 and H3K27me1 methylation levels (Ikeda et al., 2017; Vongs et al., 1993; Zemach et al., 2013), whereas silencing defects in *mom1* mutants occur without major changes in these epigenetic marks (Amedeo et al., 2000; Habu et al., 2006; Han et al., 2016; Moissiard et al., 2014; Vaillant et al., 2006).

We identified 1909 and 94 TEs significantly upregulated in *ddm1-2* and *mom1-2*, respectively. Most TEs derepressed in *mom1-2* overlapped with those derepressed in the *ddm1-2* mutants (figure 5A), consistent with MOM1 targeting a subset of methylated TEs for silencing. Overall, TEs upregulated in *ddm1-2* accumulated slightly decreased transcript levels in *med14-3 ddm1-2* and weakly increased transcript levels

in *uvh6-4 ddm1-2* (supplementary figure 10A). Interestingly, TEs derepressed by the *mom1-2* mutation showed strong reduction of transcript levels in *med14-3 mom1-2* (supplementary figure 10B). Although not statistically significant, TE upregulation tend to be stronger in *uvh6-4 mom1-2*. This suggests a strong dependency over MED14 for TE transcription in *mom1-2*, whereas TE transcription in the *ddm1-2* background is mostly independent of MED14. To strengthen this conclusion, we narrowed down the analysis to the TEs commonly derepressed by both *ddm1-2* and *mom1-2* mutations. Again, at these 78 TEs, *med14-3* and *uvh6-4* mutations had no significant impact on *ddm1*-induced release of silencing, whereas transcript levels in *med14-3 mom1-2* were strongly reduced relative to *mom1-2* but not in *uvh6-4 mom1-2* (figure 5B). Because DNA and H3K9me2/K27me1 methylation levels are largely reduced in *ddm1-2*, while being mostly unaltered in *mom1-2* (supplementary figure 10C) (Amedeo et al., 2000; Habu et al., 2006; Han et al., 2016; Moissiard et al., 2014; Vaillant et al., 2006), our data suggest that, upon silencing destabilization, MED14 is involved in transcription at a subset of heterochromatic TEs and requires DDM1-mediated epigenetic marks for its function. Supporting a role for DNA methylation in MED14 function, RT-qPCR assays showed that silencing release of *MULE* and *TSI* in the DNA hypomethylated *met1-3* background was not suppressed by the *med14-3* mutation (figure 5C). Remarkably, when considering TEs upregulated by heat stress, TEs depending on MED14 for transcriptional upregulation showed higher DNA methylation levels at all cytosine contexts compared to those independent of the *med14-3* mutation (figure 5D, supplementary figure 10D). Such strong bias for highly methylated elements was not observed at TEs that depended on *UVH6* for heat stress-induced transcriptional upregulation (supplementary figure 10E). Furthermore, TEs transcribed in the WT in the absence of stress and downregulated by *med14-3* were more methylated than those unaffected by the *med14-3* mutation (figure 5E).

Therefore, we conclude that MED14 promotes transcript accumulation at a set of highly methylated TEs and requires proper DNA methylation patterns for this function. On the other hand, UVH6 is required for transcription in a heat stress-specific manner and appears to show a less pronounced preference than MED14 for highly methylated TEs.

MED14 regulates non-CG DNA methylation

We sought to determine whether *med14* mutation affect DNA methylation by profiling genome-wide DNA methylation levels in WT and *med14-3* seedlings by BS-seq. Overall, DNA methylation levels were mostly unaltered at CG sites, and showed a moderate reduction at non-CG sites in *med14* compared with the WT (figure 6A). Calculating average methylation levels along all genomic PCGs, euchromatic TEs and pericentromeric TEs revealed that non-CG methylation was specifically decreased at pericentromeric TEs in *med14-3* (supplementary figure 11A, B). Because low variations on average methylation levels could mask strong changes at a limited number of loci, we divided the genome in 100-bp bins and determined differentially methylation regions (DMRs) in *med14-3* relative to the WT. This analysis confirmed that the *med14-3* mutation predominantly induced a decrease in DNA methylation at non-CG sites, and preferentially alters methylation of pericentromeric regions of the chromosomes (figure 6B, C). CHG and CHH hypomethylation occurred concurrently (supplementary figure 11C) indicating that MED14 regulates non-CG methylation at these loci.

The Mediator complex is involved in initiation of Pol II transcription and Pol II has been reported to be involved in a pathway that regulates DNA methylation (Stroud et al., 2013). Furthermore, at several heterochromatic loci, Mediator promotes Pol II-mediated production of long noncoding scaffold RNAs, which

serve to recruit Pol V to these loci (Kim et al., 2011). To assess whether MED14 and Pol II regulate DNA methylation at the same loci, we determined DNA methylation levels of *med14* hypomethylated DMRs in the *nrpb2-3* Pol II mutant allele using previously published data (Zhai et al., 2015). For the vast majority of these genomic regions, DNA methylation levels were unaltered in *nrpb2-3* (supplementary figure 12A), indicating that MED14 regulates DNA methylation largely independently of Pol II.

In the Arabidopsis genome, CHG methylation is mostly mediated by the H3K9me2-directed CMT3 chromomethylase, while CHH methylation is maintained by CMT2 and the RdDM pathway at largely distinct genomic regions (Stroud et al., 2014; Zemach et al., 2013). RdDM requires the production of noncoding RNAs by Pol IV and Pol V, which are eventually required to target and recruit the RdDM effector complex containing the DRM2 *de novo* methyltransferase to its genomic targets (Matzke and Mosher, 2014). We used published data (Stroud et al., 2013) to determine non-CG methylation levels at *med14* non-CG hypomethylated DMRs in mutants for CMT3, CMT2, Pol IV (NRPD1), Pol V (NRPE1) and DRM1/2. *med14* CHG hypomethylated DMRs showed nearly WT methylation levels in *cmt2*, whereas they were largely hypomethylated in *cmt3* (supplementary figure 12B), in agreement with the prominent role of CMT3 over CMT2 in controlling CHG methylation (Stroud et al., 2014). Interestingly, many *med14* CHG hypo DMRs showed reduced DNA methylation level in the *nrpd1, nrpe1* and *drm1/2* RdDM mutants (supplementary figure 12B). Strikingly, *med14* CHH hypomethylated DMRs showed strongly reduced DNA methylation level in these RdDM mutants (figure 6D). This was not merely due to a genome-wide impact of RdDM deficiency on CHH methylation since the same number of randomly selected genomic regions showed much less reduction in CHH methylation in the RdDM mutants (figure 6E). Conversely, loci with reduced CHH methylation in *drm1/2*, *nrpd1* or *nrpe1* all showed lower CHH methylation in *med14-3* (supplementary figure 12C). Together, these results indicate that MED14 regulates non-CG methylation at a subset of loci, likely through RdDM.

Discussion

Previous studies have shown that heat stress or mutations in certain silencing factors can trigger heterochromatin transcription without modifying levels of repressive epigenetic marks (Amedeo et al., 2000; Lang-Mladek et al., 2010; Moissiard et al., 2012; Pecinka et al., 2010; Tittel-Elmer et al., 2010). That transcription could occur in an otherwise repressive environment suggested that specific mechanisms were involved (Tittel-Elmer et al., 2010). Here, we identified MED14 and UVH6 as critical factors for heterochromatin transcription during heat stress. We showed that UVH6 is dispensable for heterochromatin transcription in silencing mutants such as *mom1* and *ddm1,* while MED14 is solely required when heterochromatic marks are not altered. Additionally, we showed that MED14 participates in maintenance of DNA methylation at a subset of RdDM-dependent loci.

XPD, the human UVH6 ortholog, is the central subunit of the TFIIH complex, which is crucial for nucleotide exchange repair and is considered a global transcription factor (Compe and Egly, 2016). Our data show that *uvh6* mutations impair transcription of many genes and TEs specifically at elevated temperature. This suggests that UVH6 is not generally required for transcription initiation in Arabidopsis, but is rather involved in a stress-specific transcription mechanism. Previous studies showed that UVH6 belongs to the most essential factors regarding thermotolerance (Jenkins et al., 1997; Larkindale et al., 2005), although the molecular pathway involved is not known. Interestingly, heat-induced accumulation of the canonical heat-

responsive factors HSFs and HSPs is independent of UVH6 (Hu et al., 2015; Larkindale et al., 2005), reinforcing the notion that UVH6 is not required for transcription of all genes during heat stress. Human TFIIH has been shown to be involved in selective transcriptional responses to various *stimuli* through post-translational modifications or recruitment of transcription factors (Chen et al., 2000; Chymkowitch et al., 2011; Compe et al., 2007; Keriel et al., 2002; Sano et al., 2007; Traboulsi et al., 2014). Therefore, UVH6 may cooperate with HSFs or other transcription factors during heat stress. In human, XPD is involved in many functions on top of its well-established roles in transcription and repair, sometimes in other complex than TFIIH (Compe and Egly, 2016). To get a better understanding of UVH6-dependent transcription in heat stress, futures efforts should try to determine if UVH6 acts as a component of the TFIIH complex or separately.

Mediator is a large protein complex organized in a head, middle and tail modules, with a transiently associated CDK8 kinase module (Soutourina, 2018). MED14 connects the three main modules and is critical for Mediator architecture and its function as a co-activator of Pol II transcription (Cevher et al., 2014). We found that MED14 preferentially stimulates transcription of highly methylated TEs in control and stressed conditions. TEs derepressed in *mom1* mutants require MED14 for transcription, and importantly, the same subset of TEs loose MED14 dependency in the DNA hypomethylated *ddm1* background. Similarly, MED14 did not stimulate transcription in a hypomethylated *met1* background. These results suggest that DNA methylation is required for MED14 targeting to heterochromatin. In yeast, the Mediator complex interacts with nucleosomes (Liu and Myers, 2012; Lorch et al., 2000; Zhu et al., 2011a) and the interaction is mediated by histone modifications, although it is not clear how (Uthe et al., 2017; Zhu et al., 2011b). Our data further indicate that MED14 controls DNA methylation at loci where DNA methylation depends on RdDM. RdDM relies on the combined production of non-coding RNAs by the Pol II-related Pol IV and Pol V (Matzke and Mosher, 2014). Compared with transcription initiation by Pol II, less is known about the factors involved in transcription initiation by Pol IV and Pol V. However, epigenetic information appears also crucial for Pol IV and Pol V targeting. Recruitment of Pol IV involves SAWADEE HOMEODOMAIN HOMOLOG 1 (SHH1), a Pol IV-interacting protein that binds to the repressive histone modification H3K9me2 (Law et al., 2013). The SU(VAR)3-9 homologues SUVH2 and SUVH9 are capable of binding methylated DNA and recruit Pol V to DNA methylation (Johnson et al., 2014). Similar to *med14, shh1* and *suvh2/9* mutations also reduce non-CG DNA methylation at a subset RdDM targets. Previous studies proposed that Pol II is required for proper DNA methylation patterns (Stroud et al., 2013) and that Mediator stimulates Pol II-mediated production of non-coding scaffold RNAs that recruits Pol V (Kim et al., 2011). However, we found that DNA methylation at MED14-controlled regions is largely independent of Pol II. Therefore, we propose that MED14 is involved in RdDM at a subset of genomic loci where it might be involved in the early steps of RdDM by acting as a co-activator of Pol IV and/or Pol V.

Although MED14 makes multiple contacts with the different Mediator modules, the C-terminal part of yeast and human MED14 has been mapped to the tail module (Nozawa et al., 2017; Tsai et al., 2014). Accordingly, C-terminal truncations of MED14 led to dissociation of the tail module in yeast (Li et al., 1995; Liu and Myers, 2012). The *med14-3* mutation isolated in our study induces a stop codon at amino acid 1090 of MED14, truncating 614 amino acids at the C-terminal end. The Mediator subunits are relatively well conserved between yeast, human and Arabidopsis (Bäckström et al., 2007). By analogy, the *med14-3* mutation reported here may be expected to lead to tail module dissociation. Interestingly, the tail module

seems important for recruiting the Mediator complex to chromatin (Jeronimo and Robert, 2017; Soutourina, 2018). Thus, the Mediator tail module may mediate the preference of MED14 for DNA methylated loci.

In fission yeast, mutations of some subunits from the Mediator head and middle modules induce defects in heterochromatin silencing at pericentromeres and concomitant loss of the heterochromatic mark H3K9me2 (Carlsten et al., 2012; Oya et al., 2013; Thorsen et al., 2012). Our transcriptomic data do not support a role for Arabidopsis Mediator in heterochromatin silencing. Heterochromatin formation in *S. pombe* is dependent on RNAi-dependent and -independent pathways that both rely on RNA molecules (Martienssen and Moazed, 2015); however, pathways that maintain heterochromatin in Arabidopsis seem largely independent of heterochromatin transcription (Law and Jacobsen, 2010). Therefore, it is possible that Mediator stimulates heterochromatin transcription in both model organisms, where it would feed heterochromatin silencing in yeast and RdDM in Arabidopsis. Interestingly, in a yeast mutant background where silencing is compromised but heterochromatin is maintained, the Med18 Mediator subunit is required for heterochromatin transcription of the silent mating-type locus (Oya et al., 2013). This is reminiscent of our observation that MED14 is required for heterochromatin transcription only when heterochromatic marks are maintained. Altogether, these findings are in agreement with a conserved role of Mediator in stimulating heterochromatin transcription.

Heterochromatin transcription, albeit originally counter-intuitive, is a widely reported phenomenon in plants, yeast, drosophila and mammals. It occurs during specific cell cycle or developmental stages and in stress conditions (Hall et al., 2012; Negi et al., 2016; Saksouk et al., 2015; Valgardsdottir et al., 2008). A well-established function of heterochromatin-derived transcripts is to stimulate heterochromatin formation and/or direct deposition of repressive epigenetic marks (Grewal and Elgin, 2007; Martienssen and Moazed, 2015). Transcripts from heterochromatic regions serve to guide the RdDM pathway in plants, the RNA-induced transcriptional silencing complex in fission yeast (Martienssen and Moazed, 2015) or the piRNA pathway in drosophila (Andersen et al., 2017; Guzzardo et al., 2013). In mammals, the role of heterochromatin transcripts in heterochromatin formation is not clear (Saksouk et al., 2015). Despite its prevalence, the mechanism of heterochromatin transcription remains poorly characterized. Our study uncovers an important role of the conserved proteins XPD/UVH6 and MED14 in this process in Arabidopsis.

Methods

Plant material

The *ddm1-2* (Vongs et al., 1993), *mom1-2* (SAIL_610_G01), *arp6-1* (Kumar and Wigge, 2010) and *atmorc6-3* (Moissiard et al., 2012) mutants are in the Columbia (Col-0) background. The *uvh6-1* mutant is in a Columbia gl1 background (gl1) (Jenkins et al., 1995). The transgenic L5 line was kindly provided by Hervé Vaucheret (Morel et al., 2000). Plants were grown in soil or *in vitro* in a growth cabinet at 23°C, 50% humidity, using long day conditions (16h light, 8h dark). For *in vitro* conditions, seeds were surface sterilized with calcium hypochlorite and sowed on solid Murashige and Skoog medium containing 1% sucrose (w/v). The RNA-seq data for *med14-3* (figure 3, 4) was generated with *med14-3* mutants backcrossed five times. For all other molecular data presented in this study, we used lines backcrossed six times for *med14-3* and *uvh6-3* and five times for *uvh6-4*. Point mutations were genotyped by dCAPS.

GUS assay

Following heat or control treatment, rosette leaves were transferred to 3ml of a staining solution composed of 400 µg/ml 5-bromo-4-chloro-3-indolyl-β-D-glucuronic acid, 10 mM EDTA, 50 mM sodium phosphate buffer pH 7.2, 0.2% triton X-100. Leaves were placed in a desiccator, subjected to void for 5 minutes two times, and subsequently incubated 20h to 24h at 37°C. Chlorophyll was then repeatedly dissolved in ethanol to allow proper staining visualization.

Mutagenesis, screening and mapping

We used EMS-mutagenized seeds from a previously described study (Ikeda et al., 2017). To screen for mutants deficient in heat stress-induced release of silencing of the *L5-GUS* transgene, one leaf per M2 plant was dissected, and leaves from four plants were heat-stressed together with a 24h incubation at 37°C in dH2O. Leaves were subsequently subjected to GUS staining as described above. To isolate mutant candidates, a second round of screening was applied to each individual of M2 pools that contained leaves with reduced GUS signal relative to the non-mutagenized progenitor L5 line.

Mapping by sequencing was performed as previously reported (Ikeda et al., 2017). Briefly, we crossed *zen* mutants with *Ler*, selected F2 segregants with a mutant phenotype (reduced GUS staining after heat stress relative to the L5 line) and bulk-extracted DNA. Libraries were sequenced on a Illumina HiSeq 2500 instrument at Fasteris S.A. (Geneva, Switzerland), generating 100 bp paired-end reads. Sequencing analysis (Ikeda et al., 2017) revealed a locus depleted in genetic markers associated with *Ler*, on chromosome 3 for *med14-3* and on chromosome 1 for *uvh6-3*. Candidate genes with EMS-induced non-synonymous mutations were identified in the mapping interval. Available mutant lines for the candidate genes were analyzed for impaired release of gene silencing upon heat stress, allowing identification of *MED14* and *UVH6*. As indicated in the result section, the *uvh6-4* mutation was identified by complementation test and Sanger sequencing.

Cloning and complementation

For the pMED14::MED14-GFP construct, the MED14 promoter was PCR amplified from Col-0 genomic DNA from positions -1311 to -205, where +1 is the adenine of the ATG start codon; the MED14 full-length complementary DNA (cDNA) was purchased from the plant genome project of RIKEN Genomic Sciences Center (Seki et al., 1998, 2002) and its stop codon was removed by PCR. The promoter and cDNA were cloned into a pBluescript SK plasmid supplemented with attP sites by BP recombination, and subsequently introduced into pB7FWG2 by LR recombination. For the p35S::MED14 construct, the MED14 cDNA was introduced by LR recombination into a pBINHygTX plasmid supplemented with attR sequences. For p35S::UVH6-GFP construct, the UVH6 cDNA without stop codon was amplified from Col-0 RNA and introduced by BP recombination into the pDONR/ZEO vector (Invitrogen). The fragment was introduced into pH7FWG2 by LR recombination. The *med14-3* and *uvh6-3* mutants were complemented by Agrobacterium-mediated transformation (Clough and Bent, 1998).

Protein sequence alignments and protein domains

Amino acid sequences were aligned with Clustal Omega v1.2.4. To determine the position of MED14 domains (figure 2G), *A. thaliana* MED14 was aligned with *S. pombe* MED14 and the domains were determined according to a *S. pombe* structural study (Tsai et al., 2017). The positions of LXXLL motifs

(where X is any amino acid), typical of transcriptional co-activators, have been represented for indicative purpose only. *A. thaliana* UVH6 was aligned with *S. cerevisiae* RAD3, *H. sapiens* XPD (supplementary figure 4) and domains were infered from a joint analysis of RAD3 and XPD (Luo et al., 2015) whereas helicase motifs coordinates sourced from a comparative study of eukaryotic and archeal XPD proteins (Wolski et al., 2008).

Heat stress and UV-C irradiation

Rosette leaves were cut with forceps and transferred to 6-well tissue culture plates containing 3ml dH2O. They were subsequently incubated for 24h in a 23°C or 37°C growth cabinet with otherwise standard conditions. For molecular analysis, nine to twelve rosette leaves from three to four seedlings were pooled for heat or control treatment. Rosette leaves were then dried on absorbent paper, flash-frozen in liquid nitrogen and stored at -80°C or directly processed.

For survival assays, seeds were sowed *in vitro*, stratified for 72h in the dark at 4°C and grown 7 days in standard conditions before heat or UV treatment. Heat stress was applied for 24h or 48h. UV-irradiation was performed in an Et-OH sterilized UV chamber (GS Gene Linker, Bio-Rad) equipped with 254 nm bulbs. Plate lids were removed before irradiation at 10 000 J / m2 and placed back immediately. Irradiated seedlings were transferred to a dark growth cabinet with standard conditions for 24h to block photoreactivation before recovering in light for five days.

RNA analysis

Total RNA was extracted in TRIzol reagent, precipitated with isopropanol and washed two times in ethanol 70%. Integrity was assessed by running 1ug of RNA through an agarose gel after RNA denaturation in 1X MOPS 4% formaldehyde for 15 minutes at 65°C. 2ug of RNA were then DNase treated using 2 unit of RQ1 DNAse (Promega) in 15ul, following manufacturer's instructions. DNase-treated RNAs were further diluted to 40ul in RNase-free H2O before subsequent analysis. 50ng of RNA was used as input for reverse transcription PCR (RT-PCR). End-point RT-PCR was performed with the one-step RT-PCR kit (Qiagen) following manufacturer's instructions in a final volume of 10ul. For 18S rRNA, MULE, 106B, TSI and 180bp, we respectively performed 20, 26, 35, 28 and 37 cycles. RT-qPCR were performed in a final volume of 10ul with the SensiFAST^{TM} SYBR® No-ROX One-Step Kit (Bioline) in an Eco Real-time PCR system (Illumina). Quantification cycle (Cq or Ct) values were analyzed following the $2^{-\Delta\Delta CT}$ method (Livak and Schmittgen, 2001). The mean of biological replicates from the control condition was subtracted to each ΔCq value to calculate ΔΔCq. Means and standard errors from biological replicates were calculated from $2^{-\Delta\Delta Cq}$ values.

mRNA-sequencing

Total RNA was extracted and treated as indicated above except that following DNase treatment, RNAs were further purified in phenol-chloroform. Sequencing libraries were generated and sequenced as 50bp single-end reads at Fasteris S.A. (Geneva, Switzerland). Read mapping and quantification of gene expression were performed as previously reported (Ikeda et al., 2017). To allow comparisons between *uvh6-3*, *med14-3* and *uvh6-4* (figure 3 and supplementary figure 6), the *uvh6-4* sample and its corresponding WT were artificially converted to non-stranded libraries by merging sense and antisense reads and re-calculating RPKM values at each locus. For comparisons of WT at 37°C versus (vs) WT at 23°C, *ddm1-2* vs WT and *mom1*-2 vs WT, differentially expressed loci (PCGs and TEs) were defined by a log2 fold change >= 1 or <= -1, a false

discovery rate (FDR) < 0.01 and only loci defined as differentially expressed in both replicates were retained. When reads could be assigned to a specific strand (*ddm1-2* and *mom1-2* libraries), differential expression was tested in both orientations for each annotation, and only loci that were differentially expressed on the same orientation in both replicates were retained. For all other comparisons, since a single replicate was analyzed, the log2 fold change threshold was increased to >= 2 or <= -2. Gene ontology analysis was performed using Panther Overrepresentation Test (05/12/2017 release) using the 27/12/2017 Gene Ontology database (Ashburner et al., 2000).

To analyze TE transcription in WT and *med14-3* in standard conditions (23°C) (figure 5E), we aligned reads from WT and *med14-3* with STAR (Dobin et al., 2013) and retained multi-mapped reads randomly assigned. We counted reads on TAIR10 transposon annotations and selected TEs with a minimum RPKM value of one in WT, a minimum length of 200 bp and that had at most 10% of their length intersecting a protein coding gene annotation, regardless of their orientation.

For transcriptomic studies of *med14-3* in the *ddm1-2* background, we compared *med14-3 ddm1-2* double mutants with *ddm1-2* mutants, both isolated from the F2 progeny of a *med14-3*/+ *ddm1-2*/+ F1 plant. We followed the same method for *uvh6-4 ddm1-2*. For *med14-3* in the *mom1-2* background, we compared *med14-3 mom1-2* double mutants with *mom1-2* mutants, both isolated from the F3 progeny of a *med14-3*/+ *mom1-2* F2 plant, and followed the same method for *uvh6-4 mom1-2*.

Whole-genome bisulfite sequencing

After 24h incubation at 23°C in dH2O of 16-day-old rosette leaves from L5 and *med14-3*, genomic DNA was extracted using the Wizard® Genomic DNA Purification Kit (Promega) following manufacturer's instructions. One microgram of DNA was used for bisulfite treatment, library preparation and sequencing on a Hiseq2000 at the Beijing Genomics Institute (Shenzhen, China), producing paired 91-bp oriented reads. We used and re-analyzed previously published BS-seq datasets for *ddm1-2* (GSM981009), *cmt2-7* (GSM981002), *cmt3-11* (GSM981003), *drm1/2* (*drm1-2 drm2-2*; GSM981015), *nrpd1a-4* (GSM981039), *nrpe1-11* (GSM981040) and WT (GSM980986) (Stroud et al., 2013); *mom1-2* (GSM1375964) and WT (GSM1375966) (Moissiard et al., 2014); *nrpb2-3* (GSM1848705, GSM1848706) and WT (GSM1848703, GSM1848704) (Zhai et al., 2015).

PCR duplicates were removed using a custom program: a read pair was considered duplicated if both reads from a pair were identical to both reads of another read pair. We utilized BS-Seeker2 v2.1.5 (Guo et al., 2013) to map libraries on the TAIR10 reference genome using the Bowtie2 aligner with 4% mismatches and call methylation values from uniquely-mapped reads. 100kb-window average methylation levels and metaplots of average methylation levels over PCGs or subgroups of TEs were generated in CG, CHG and CHH contexts with CGmapTools v0.1.0 (Guo et al., 2018). For metaplots, regions of interest were divided in 40 bins of equal length while upstream and downstream regions extended for 30 bins of 100 base pairs.

DMRs were calculated as previously reported (Stroud et al., 2013), except that contiguous DMRs were not merged, and that the thresholds for minimum methylation differences were 0.4, 0.2 and 0.2 for respectively CG, CHG and CHH contexts. To extract methylation levels at specific regions (e.g. figure 5D, 6D), we first calculated the methylation level of individual cytosines in the region and extracted the average. For all calculations of methylation levels or DMRs, only cytosines with a minimum coverage of 6 reads were considered.

Statistical analysis

Means and standard errors of the mean were calculated from independent biological samples. All analysis were conducted with R version 3.4.0 (R Core Team, 2017). All boxplots had whiskers extend to the furthest data point that is less than 1.5 fold interquartile range from the box (Tukey's definition). Heatmaps were generated using the *heatmap.2* function of the *gplots* package with euclidean distance, complete clustering and without scaling (Warnes et al., 2005). Differences in mean for RT-qPCR data were tested using an unpaired Student's t-test with Welch's correction with the *t.test* function. For RT-qPCR data in supplementary figure 9, because of the interaction between the temperature treatments and genotypes, the data was split between 23°C and 37°C. Subsequent analysis of variance was performed with the *aov* function, and *post-hoc* analysis was performed with Tukey's Honest Significant Difference (HSD) test, using the *TukeyHSD* function with a 95% confidence level. Since the strong absolute variance of WT at 37°C prohibited the assessment of differences between mutants, this sample was excluded. Differences in distributions of RPKM values (figure 5B; supplementary figure 6A, 10A, 10B) and methylation values (figure 5D, 5E; supplementary figure 12C) were tested with an unpaired two-sided Mann-Whitney test using the *wilcox.test* function.

References

Amedeo, P., Habu, Y., Afsar, K., Scheid, O.M., and Paszkowski, J. (2000). Disruption of the plant gene MOM releases transcriptional silencing of methylated genes. Nature *405*, 203–206.

Andersen, P.R., Tirian, L., Vunjak, M., and Brennecke, J. (2017). A heterochromatin-dependent transcription machinery drives piRNA expression. Nature *549*, 54–59.

Ashburner, M., Ball, C.A., Blake, J.A., Botstein, D., Butler, H., Cherry, J.M., Davis, A.P., Dolinski, K., Dwight, S.S., Eppig, J.T., et al. (2000). Gene Ontology: tool for the unification of biology. Nat. Genet. *25*, 25–29.

Autran, D., Jonak, C., Belcram, K., Beemster, G.T.S., Kronenberger, J., Grandjean, O., Inzé, D., and Traas, J. (2002). Cell numbers and leaf development in Arabidopsis: a functional analysis of the STRUWWELPETER gene. EMBO J. *21*, 6036–6049.

Bäckström, S., Elfving, N., Nilsson, R., Wingsle, G., and Björklund, S. (2007). Purification of a Plant Mediator from Arabidopsis thaliana Identifies PFT1 as the Med25 Subunit. Mol. Cell *26*, 717–729.

Carlsten, J.O., Szilagyi, Z., Liu, B., Lopez, M.D., Szaszi, E., Djupedal, I., Nystrom, T., Ekwall, K., Gustafsson, C.M., and Zhu, X. (2012). Mediator Promotes CENP-A Incorporation at Fission Yeast Centromeres. Mol. Cell. Biol. *32*, 4035–4043.

Castel, S.E., and Martienssen, R.A. (2013). RNA interference in the nucleus: roles for small RNAs in transcription, epigenetics and beyond. Nat. Rev. Genet. *14*, 100–112.

Cavrak, V. V, Lettner, N., Jamge, S., Kosarewicz, A., Bayer, L.M., and Mittelsten Scheid, O. (2014). How a Retrotransposon Exploits the Plant's Heat Stress Response for Its Activation. PLoS Genet. *10*, e1004115.

Cevher, M.A., Shi, Y., Li, D., Chait, B.T., Malik, S., and Roeder, R.G. (2014). Reconstitution of active human core Mediator complex reveals a critical role of the MED14 subunit. Nat. Struct. Mol. Biol. *21*, 1028–1034.

Chan, F.L., and Wong, L.H. (2012). Transcription in the maintenance of centromere chromatin identity. Nucleic Acids Res. *40*, 11178–11188.

Chen, D., Riedl, T., Washbrook, E., Pace, P.E., Coombes, R.C., Egly, J.M., and Ali, S. (2000). Activation of estrogen receptor alpha by S118 phosphorylation involves a ligand-dependent interaction with TFIIH and participation of CDK7. Mol. Cell *6*, 127–137.

Chymkowitch, P., Le May, N., Charneau, P., Compe, E., and Egly, J.-M. (2011). The phosphorylation of the androgen receptor by TFIIH directs the ubiquitin/proteasome process. EMBO J. *30*, 468–479.

Clough, S.J., and Bent, A.F. (1998). Floral dip: a simplified method forAgrobacterium-mediated transformation ofArabidopsis thaliana. Plant J. *16*, 735–743.

Compe, E., and Egly, J.-M. (2012). TFIIH: when transcription met DNA repair. Nat. Rev. Mol. Cell Biol. *13*, 343–354.

Compe, E., and Egly, J.-M. (2016). Nucleotide Excision Repair and Transcriptional Regulation: TFIIH and Beyond. Annu. Rev. Biochem. *85*, 265–290.

Compe, E., Malerba, M., Soler, L., Marescaux, J., Borrelli, E., and Egly, J.-M. (2007). Neurological defects in trichothiodystrophy reveal a coactivator function of TFIIH. Nat. Neurosci. *10*, 1414–1422.

Dobin, A., Davis, C.A., Schlesinger, F., Drenkow, J., Zaleski, C., Jha, S., Batut, P., Chaisson, M., and Gingeras, T.R. (2013). STAR: ultrafast universal RNA-seq aligner. Bioinformatics *29*, 15–21.

Du, J., Zhong, X., Bernatavichute, Y. V, Stroud, H., Feng, S., Caro, E., Vashisht, A.A., Terragni, J., Chin, H.G., Tu, A., et al. (2012). Dual Binding of Chromomethylase Domains to H3K9me2-Containing Nucleosomes Directs DNA Methylation in Plants. Cell *151*, 167–180.

Elmayan, T., Proux, F., and Vaucheret, H. (2005). Arabidopsis RPA2: A Genetic Link among Transcriptional Gene Silencing, DNA Repair, and DNA Replication. Curr. Biol. *15*, 1919–1925.

Feng, W., and Michaels, S.D. (2015). Accessing the Inaccessible: The Organization, Transcription, Replication, and Repair of Heterochromatin in Plants. Annu. Rev. Genet. *49*, 439–459.

Feng, S., Cokus, S.J., Schubert, V., Zhai, J., Pellegrini, M., and Jacobsen, S.E. (2014). Genome-wide Hi-C Analyses in Wild-Type and Mutants Reveal High-Resolution Chromatin Interactions in Arabidopsis. Mol. Cell *55*, 694–707.

Gonzalez, D., Bowen, A.J., Carroll, T.S., and Conlan, R.S. (2007). The Transcription Corepressor LEUNIG Interacts with the Histone Deacetylase HDA19 and Mediator Components MED14 (SWP) and CDK8 (HEN3) To Repress Transcription. Mol. Cell. Biol. *27*, 5306–5315.

Grewal, S.I.S., and Elgin, S.C.R. (2007). Transcription and RNA interference in the formation of heterochromatin. Nature *447*, 399–406.

Guo, W., Fiziev, P., Yan, W., Cokus, S., Sun, X., Zhang, M.Q., Chen, P.-Y., and Pellegrini, M. (2013). BS-Seeker2: a versatile aligning pipeline for bisulfite sequencing data. BMC Genomics *14*, 774.

Guo, W., Zhu, P., Pellegrini, M., Zhang, M.Q., Wang, X., and Ni, Z. (2018). CGmapTools improves the precision of heterozygous SNV calls and supports allele-specific methylation detection and visualization in bisulfite-sequencing data. Bioinformatics *34*, 381–387.

Guzzardo, P.M., Muerdter, F., and Hannon, G.J. (2013). The piRNA pathway in flies: highlights and future directions. Curr. Opin. Genet. Dev. *23*, 44–52.

Habu, Y., Mathieu, O., Tariq, M., Probst, A. V, Smathajitt, C., Zhu, T., and Paszkowski, J. (2006). Epigenetic regulation of transcription in intermediate heterochromatin. EMBO Rep. *7*, 1279–1284.

Hall, L.E., Mitchell, S.E., and O'Neill, R.J. (2012). Pericentric and centromeric transcription: a perfect balance required. Chromosom. Res. *20*, 535–546.

Han, Y.-F., Zhao, Q.-Y., Dang, L.-L., Luo, Y.-X., Chen, S.-S., Shao, C.-R., Huang, H.-W., Li, Y.-Q., Li, L., Cai, T., et al. (2016). The SUMO E3 Ligase-Like Proteins PIAL1 and PIAL2 Interact with MOM1 and Form a Novel Complex Required for Transcriptional Silencing. PLANT CELL ONLINE *28*, 1215–1229.

Hemsley, P.A., Hurst, C.H., Kaliyadasa, E., Lamb, R., Knight, M.R., De Cothi, E.A., Steele, J.F., and Knight, H. (2014). The Arabidopsis Mediator Complex Subunits MED16, MED14, and MED2 Regulate Mediator and RNA Polymerase II Recruitment to CBF-Responsive Cold-Regulated Genes. Plant Cell *26*, 465–484.

Hu, Z., Song, N., Zheng, M., Liu, X., Liu, Z., Xing, J., Ma, J., Guo, W., Yao, Y., Peng, H., et al. (2015). Histone acetyltransferase GCN5 is essential for heat stress-responsive gene activation and thermotolerance in Arabidopsis. Plant J. *84*, 1178–1191.

Huang, Y.-C., Niu, C.-Y., Yang, C.-R., and Jinn, T.-L. (2016). The heat-stress factor HSFA6b connects ABA signaling and ABA-mediated heat responses. Plant Physiol. *172*, pp.00860.2016.

Ikeda, Y., Pélissier, T., Bourguet, P., Becker, C., Pouch-Pélissier, M.-N., Pogorelcnik, R., Weingartner, M., Weigel, D., Deragon, J.-M., and Mathieu, O. (2017). Arabidopsis proteins with a transposon-related domain act in gene silencing. Nat. Commun. *8*, 15122.

Ito, H., Gaubert, H., Bucher, E., Mirouze, M., Vaillant, I., and Paszkowski, J. (2011). An siRNA pathway prevents transgenerational retrotransposition in plants subjected to stress. Nature *472*, 115–119.

Iwasaki, M., and Paszkowski, J. (2014). Identification of genes preventing transgenerational transmission of stress-induced epigenetic states. Proc. Natl. Acad. Sci. *111*, 8547–8552.

Jacob, Y., Feng, S., LeBlanc, C.A., Bernatavichute, Y. V, Stroud, H., Cokus, S., Johnson, L.M., Pellegrini, M., Jacobsen, S.E., and Michaels, S.D. (2009). ATXR5 and ATXR6 are H3K27 monomethyltransferases required for chromatin structure and gene silencing. Nat. Struct. Mol. Biol. *16*, 763–768.

Jansen, M.A.., Gaba, V., and Greenberg, B.M. (1998). Higher plants and UV-B radiation: balancing damage, repair and acclimation. Trends Plant Sci. *3*, 131–135.

Jenkins, M.E., Harlow, G.R., Liu, Z., Shotwell, M.A., Ma, J., and Mount, D.W. (1995). Radiation-sensitive mutants of Arabidopsis thaliana. Genetics *140*, 725–732.

Jenkins, M.E., Suzuki, T.C., and Mount, D.W. (1997). Evidence that heat and ultraviolet radiation activate a common stress-response program in plants that is altered in the uvh6 mutant of Arabidopsis thaliana. Plant Physiol. *115*, 1351–1358.

Jeronimo, C., and Robert, F. (2017). The Mediator Complex: At the Nexus of RNA Polymerase II Transcription. Trends Cell Biol. *27*, 765–783.

Johnson, L.M., Du, J., Hale, C.J., Bischof, S., Feng, S., Chodavarapu, R.K., Zhong, X., Marson, G., Pellegrini, M., Segal, D.J., et al. (2014). SRA- and SET-domain-containing proteins link RNA polymerase V occupancy to DNA methylation. Nature *507*, 124–128.

Kanno, T., Mette, M.F., Kreil, D.P., Aufsatz, W., Matzke, M., and Matzke, A.J.M. (2004). Involvement of Putative SNF2 Chromatin Remodeling Protein DRD1 in RNA-Directed DNA Methylation. Curr. Biol. *14*, 801–805.

Kapoor, A., Agarwal, M., Andreucci, A., Zheng, X., Gong, Z., Hasegawa, P.M., Bressan, R.A., and Zhu, J.-K. (2005). Mutations in a conserved replication protein suppress transcriptional gene silencing in a DNA-methylation-independent manner in Arabidopsis. Curr. Biol. *15*, 1912–1918.

Keriel, A., Stary, A., Sarasin, A., Rochette-Egly, C., and Egly, J.M. (2002). XPD mutations prevent TFIIH-dependent transactivation by nuclear receptors and phosphorylation of RARalpha. Cell *109*, 125–135.

Kim, Y.J., Zheng, B., Yu, Y., Won, S.Y., Mo, B., and Chen, X. (2011). The role of Mediator in small and long noncoding RNA production in Arabidopsis thaliana. EMBO J. *30*, 814–822.

Kumar, S.V., and Wigge, P.A. (2010). H2A.Z-Containing Nucleosomes Mediate the Thermosensory Response in Arabidopsis. Cell *140*, 136–147.

Kunz, B.A., Anderson, H.J., Osmond, M.J., and Vonarx, E.J. (2005). Components of nucleotide excision repair and DNA damage tolerance in Arabidopsis thaliana. Environ. Mol. Mutagen. *45*, 115–127.

Lang-Mladek, C., Popova, O., Kiok, K., Berlinger, M., Rakic, B., Aufsatz, W., Jonak, C., Hauser, M.-T., and

Luschnig, C. (2010). Transgenerational inheritance and resetting of stress-induced loss of epigenetic gene silencing in Arabidopsis. Mol. Plant *3*, 594–602.

Larkindale, J., Hall, J.D., Knight, M.R., and Vierling, E. (2005). Heat stress phenotypes of Arabidopsis mutants implicate multiple signaling pathways in the acquisition of thermotolerance. Plant Physiol. *138*, 882–897.

Law, J.A., and Jacobsen, S.E. (2010). Establishing, maintaining and modifying DNA methylation patterns in plants and animals. Nat. Rev. Genet. *11*, 204–220.

Law, J.A., Du, J., Hale, C.J., Feng, S., Krajewski, K., Palanca, A.M.S., Strahl, B.D., Patel, D.J., and Jacobsen, S.E. (2013). Polymerase IV occupancy at RNA-directed DNA methylation sites requires SHH1. Nature *498*, 385–389.

Li, Y., Bjorklund, S., Jiang, Y.W., Kim, Y.J., Lane, W.S., Stillman, D.J., and Kornberg, R.D. (1995). Yeast global transcriptional regulators Sin4 and Rgr1 are components of mediator complex/RNA polymerase II holoenzyme. Proc. Natl. Acad. Sci. *92*, 10864–10868.

Liu, Z., and Myers, L.C. (2012). Med5(Nut1) and Med17(Srb4) Are Direct Targets of Mediator Histone H4 Tail Interactions. PLoS One *7*, e38416.

Liu, Z., Hong, S.W., Escobar, M., Vierling, E., Mitchell, D.L., Mount, D.W., and Hall, J.D. (2003). Arabidopsis UVH6, a homolog of human XPD and yeast RAD3 DNA repair genes, functions in DNA repair and is essential for plant growth. Plant Physiol *132*, 1405–1414.

Livak, K.J., and Schmittgen, T.D. (2001). Analysis of relative gene expression data using real-time quantitative PCR and the 2(-Delta Delta C(T)) Method. Methods *25*, 402–408.

Lorch, Y., Beve, J., Gustafsson, C.M., Myers, L.C., and Kornberg, R.D. (2000). Mediator-Nucleosome Interaction. Mol. Cell *6*, 197–201.

Luo, J., Cimermancic, P., Viswanath, S., Ebmeier, C.C., Kim, B., Dehecq, M., Raman, V., Greenberg, C.H., Pellarin, R., Sali, A., et al. (2015). Architecture of the Human and Yeast General Transcription and DNA Repair Factor TFIIH. Mol. Cell *59*, 794–806.

Martienssen, R., and Moazed, D. (2015). RNAi and Heterochromatin Assembly. Cold Spring Harb. Perspect. Biol. *7*, a019323.

Matzke, M.A., and Mosher, R.A. (2014). RNA-directed DNA methylation: an epigenetic pathway of increasing complexity. Nat. Rev. Genet. *15*, 394–408.

Moissiard, G., Cokus, S.J., Cary, J., Feng, S., Billi, A.C., Stroud, H., Husmann, D., Zhan, Y., Lajoie, B.R., McCord, R.P., et al. (2012). MORC family ATPases required for heterochromatin condensation and gene silencing. Science *336*, 1448–1451.

Moissiard, G., Bischof, S., Husmann, D., Pastor, W.A., Hale, C.J., Yen, L., Stroud, H., Papikian, A., Vashisht, A.A., Wohlschlegel, J.A., et al. (2014). Transcriptional gene silencing by Arabidopsis microrchidia homologues involves the formation of heteromers. Proc. Natl. Acad. Sci. U. S. A. *111*, 7474–7479.

Morel, J.-B., Mourrain, P., Béclin, C., and Vaucheret, H. (2000). DNA methylation and chromatin structure affect transcriptional and post-transcriptional transgene silencing in Arabidopsis. Curr. Biol. *10*, 1591–1594.

Negi, P., Rai, A.N., and Suprasanna, P. (2016). Moving through the Stressed Genome: Emerging Regulatory Roles for Transposons in Plant Stress Response. Front. Plant Sci. *7*, 1448.

Nozawa, K., Schneider, T.R., and Cramer, P. (2017). Core Mediator structure at 3.4 Å extends model of transcription initiation complex. Nature *545*, 248–251.

Oya, E., Kato, H., Chikashige, Y., Tsutsumi, C., Hiraoka, Y., and Murakami, Y. (2013). Mediator Directs Co-

transcriptional Heterochromatin Assembly by RNA Interference-Dependent and -Independent Pathways. PLoS Genet. *9*, e1003677.

Pecinka, A., Dinh, H.Q., Baubec, T., Rosa, M., Lettner, N., and Mittelsten Scheid, O. (2010). Epigenetic regulation of repetitive elements is attenuated by prolonged heat stress in Arabidopsis. Plant Cell *22*, 3118–3129.

Probst, A. V., Fransz, P.F., Paszkowski, J., and Scheid, O.M. (2003). Two means of transcriptional reactivation within heterochromatin. Plant J. *33*, 743–749.

R Core Team (2017). R: A language and environment for statistical computing. R Found. Stat. Comput. Vienna, Austria. URL Http//Www.R-Project.Org/.

Saksouk, N., Simboeck, E., and Déjardin, J. (2015). Constitutive heterochromatin formation and transcription in mammals. Epigenetics Chromatin *8*, 3.

Sakuma, Y., Maruyama, K., Qin, F., Osakabe, Y., Shinozaki, K., and Yamaguchi-Shinozaki, K. (2006). Dual function of an Arabidopsis transcription factor DREB2A in water-stress-responsive and heat-stress-responsive gene expression. Proc. Natl. Acad. Sci. *103*, 18822–18827.

Sanchez, D.H., and Paszkowski, J. (2014). Heat-induced release of epigenetic silencing reveals the concealed role of an imprinted plant gene. PLoS Genet. *10*, e1004806.

Sano, M., Izumi, Y., Helenius, K., Asakura, M., Rossi, D.J., Xie, M., Taffet, G., Hu, L., Pautler, R.G., Wilson, C.R., et al. (2007). Ménage-à-trois 1 is critical for the transcriptional function of PPARgamma coactivator 1. Cell Metab. *5*, 129–142.

Schramm, F., Larkindale, J., Kiehlmann, E., Ganguli, A., Englich, G., Vierling, E., and Von Koskull-Döring, P. (2007). A cascade of transcription factor DREB2A and heat stress transcription factor HsfA3 regulates the heat stress response of Arabidopsis. Plant J. *53*, 264–274.

Seki, M., Carninci, P., Nishiyama, Y., Hayashizaki, Y., and Shinozaki, K. (1998). High-efficiency cloning of Arabidopsis full-length cDNA by biotinylated CAP trapper. Plant J. *15*, 707–720.

Seki, M., Narusaka, M., Kamiya, A., Ishida, J., Satou, M., Sakurai, T., Nakajima, M., Enju, A., Akiyama, K., Oono, Y., et al. (2002). Functional annotation of a full-length Arabidopsis cDNA collection. Science *296*, 141–145.

Soutourina, J. (2018). Transcription regulation by the Mediator complex. Nat. Rev. Mol. Cell Biol. *19*, 262–274.

Stroud, H., Greenberg, M.V.C., Feng, S., Bernatavichute, Y. V, and Jacobsen, S.E. (2013). Comprehensive analysis of silencing mutants reveals complex regulation of the Arabidopsis methylome. Cell *152*, 352–364.

Stroud, H., Do, T., Du, J., Zhong, X., Feng, S., Johnson, L., Patel, D.J., and Jacobsen, S.E. (2014). Non-CG methylation patterns shape the epigenetic landscape in Arabidopsis. Nat. Struct. Mol. Biol. *21*, 64–72.

Takeda, S., Tadele, Z., Hofmann, I., Probst, A. V, Angelis, K.J., Kaya, H., Araki, T., Mengiste, T., Mittelsten Scheid, O., Shibahara, K., et al. (2004). BRU1, a novel link between responses to DNA damage and epigenetic gene silencing in Arabidopsis. Genes Dev. *18*, 782–793.

Thorsen, M., Hansen, H., Venturi, M., Holmberg, S., and Thon, G. (2012). Mediator regulates non-coding RNA transcription at fission yeast centromeres. Epigenetics Chromatin *5*, 19.

Tittel-Elmer, M., Bucher, E., Broger, L., Mathieu, O., Paszkowski, J., and Vaillant, I. (2010). Stress-induced activation of heterochromatic transcription. PLoS Genet. *6*, e1001175.

Traboulsi, H., Davoli, S., Catez, P., Egly, J.-M., and Compe, E. (2014). Dynamic Partnership between TFIIH, PGC-1α and SIRT1 Is Impaired in Trichothiodystrophy. PLoS Genet. *10*, e1004732.

Tsai, K.-L., Tomomori-Sato, C., Sato, S., Conaway, R.C., Conaway, J.W., and Asturias, F.J. (2014). Subunit Architecture and Functional Modular Rearrangements of the Transcriptional Mediator Complex. Cell *158*, 463.

Tsai, K.-L., Yu, X., Gopalan, S., Chao, T.-C., Zhang, Y., Florens, L., Washburn, M.P., Murakami, K., Conaway, R.C., Conaway, J.W., et al. (2017). Mediator structure and rearrangements required for holoenzyme formation. Nature *544*, 196–201.

Uthe, H., Vanselow, J.T., and Schlosser, A. (2017). Proteomic Analysis of the Mediator Complex Interactome in Saccharomyces cerevisiae. Sci. Rep. *7*, 575.

Vaillant, I., Schubert, I., Tourmente, S., and Mathieu, O. (2006). MOM1 mediates DNA-methylation-independent silencing of repetitive sequences in Arabidopsis. EMBO Rep. *7*, 1273–1278.

Valgardsdottir, R., Chiodi, I., Giordano, M., Rossi, A., Bazzini, S., Ghigna, C., Riva, S., and Biamonti, G. (2008). Transcription of Satellite III non-coding RNAs is a general stress response in human cells. Nucleic Acids Res. *36*, 423–434.

Vongs, A., Kakutani, T., Martienssen, R.A., and Richards, E.J. (1993). Arabidopsis thaliana DNA methylation mutants. Science *260*, 1926–1928.

Wang, C., Du, X., and Mou, Z. (2016). The Mediator Complex Subunits MED14, MED15, and MED16 Are Involved in Defense Signaling Crosstalk in Arabidopsis. Front. Plant Sci. *7*, 1947.

Wang, L.-C., Wu, J.-R., Chang, W.-L., Yeh, C.-H., Ke, Y.-T., Lu, C.-A., and Wu, S.-J. (2013). Arabidopsis HIT4 encodes a novel chromocentre-localized protein involved in the heat reactivation of transcriptionally silent loci and is essential for heat tolerance in plants. J. Exp. Bot. *64*, 1689–1701.

Wang, L.-C., Wu, J.-R., Hsu, Y.-J., and Wu, S.-J. (2015). Arabidopsis HIT4, a regulator involved in heat-triggered reorganization of chromatin and release of transcriptional gene silencing, relocates from chromocenters to the nucleolus in response to heat stress. New Phytol. *205*, 544–554.

Warnes, G., Bolker, B., Bonebakker, L., Gentleman, R., Huber, W., Liaw, A., Lumley, T., Mächler, M., Magnusson, A., and Möller, S. (2005). gplots: Various R programming tools for plotting data. R Packag. Version *2*.

Wendte, J.M., and Pikaard, C.S. (2017). The RNAs of RNA-directed DNA methylation. Biochim. Biophys. Acta - Gene Regul. Mech. *1860*, 140–148.

Wolski, S.C., Kuper, J., Hänzelmann, P., Truglio, J.J., Croteau, D.L., Houten, B. Van, and Kisker, C. (2008). Crystal Structure of the FeS Cluster–Containing Nucleotide Excision Repair Helicase XPD. PLoS Biol. *6*, e149.

Zemach, A., Kim, M.Y., Hsieh, P.-H., Coleman-Derr, D., Eshed-Williams, L., Thao, K., Harmer, S.L., and Zilberman, D. (2013). The Arabidopsis nucleosome remodeler DDM1 allows DNA methyltransferases to access H1-containing heterochromatin. Cell *153*, 193–205.

Zhai, J., Bischof, S., Wang, H., Feng, S., Lee, T., Teng, C., Chen, X., Park, S.Y., Liu, L., Gallego-Bartolome, J., et al. (2015). A One Precursor One siRNA Model for Pol IV-Dependent siRNA Biogenesis. Cell *163*, 445–455.

Zhang, X., Yao, J., Zhang, Y., Sun, Y., and Mou, Z. (2013). The Arabidopsis Mediator complex subunits MED14/SWP and MED16/SFR6/IEN1 differentially regulate defense gene expression in plant immune responses. Plant J. *75*, 484–497.

Zhu, X., Liu, B., Carlsten, J.O.P., Beve, J., Nystrom, T., Myers, L.C., and Gustafsson, C.M. (2011a). Mediator Influences Telomeric Silencing and Cellular Life Span. Mol. Cell. Biol. *31*, 2413–2421.

Zhu, X., Zhang, Y., Bjornsdottir, G., Liu, Z., Quan, A., Costanzo, M., Dávila López, M., Westholm, J.O., Ronne, H., Boone, C., et al. (2011b). Histone modifications influence mediator interactions with chromatin. Nucleic Acids Res. *39*, 8342–8354.

Acknowledgments

We are grateful to Korbinian Schneeberger for his help with mapping-by-sequencing. We thank Jerzy Paszkowski for his support at the early steps of this project. This work was supported by CNRS, Inserm, Université Clermont Auvergne, Young Researcher grants from the Auvergne Regional Council (to I.V. and to O.M.), an EMBO Young Investigator award (to O.M.), and a grant from the European Research Council (ERC, I2ST 260742 to O.M.). P.B. was supported by a PhD studentship from the Ministère de l'éducation nationale, de l'enseignement supérieur et de la recherche.

Author contributions

MNP and IV performed the screening and isolated the *uvh6-3* and *med14-3* mutations. MNP and IV backcrossed and outcrossed the mutants and isolated samples for mapping-by-sequencing. MNP isolated and backcrossed the *uvh6-4* mutation. TP generated the RT-qPCR data for supplementary figure 1. AD complemented the *med14-3* mutation and generated *med14-3* single mutant mRNA-seq data. LLG generated the BS-seq data for *med14-3* and the RT-qPCR data for figure 5C. AD, LLG and AGZ characterized the *med14-3* mutation with help from MNP. SdB characterized the *uvh6* mutations, and generated *uvh6-3* single mutant mRNA-seq data. PB generated all other data. RP contributed bioinformatic tools for genomic data analyses. OM and PB analyzed the genomic data, with contributions from RP and SdB. PB generated the figures with contributions from OM. PB and OM wrote the manuscript with contributions from SdB, IV and AGZ. OM and IV initially conceived the screening and TP contributed the original idea of screening isolated leaves. OM supervised the study.

Figure legends

Figure 1

A. Scheme representing the method used to submit rosette leaves to a control stress (23°C) or a heat stress (37°C). The *L5-GUS* transgene is reactivated in leaves subjected to heat stress.

B. RT-qPCR analysis of transcripts from *MULE-AT2G15810* and the *L5-GUS* transgene in L5 transgenic plants at 23°C or 37°C, normalized to the reference gene *AT5G12240* and further normalized to the mean of L5 samples at 23°C. Error bars represent standard error of the mean across three biological replicates.

C. RT-PCR analysis of transcripts from endogenous repeats in L5 transgenic plants at 23°C or 37°C. Amplification of 18S rRNAs was used as a loading control. PCR in the absence of reverse transcription (RT-) was performed to control for genomic DNA contamination.

D. (top) Transcriptional changes in WT plants subjected to heat stress represented along chromosomes by log2 ratios (37°C / 23°C) of mean RPKM values in 100kb windows. (bottom) Density of TEs detected as significantly upregulated in WT plants subjected to heat stress is plotted in red (left y axis) with total TE density in grey (right y axis), both calculated by 100 kb windows. Windows containing upregulated *ONSEN* elements (*AtCOPIA78*) are marked with an asterisk.

E. Average cytosine methylation levels by 500kb windows calculated in CG, CHG and CHH contexts in a WT subjected to a control stress (23°C) or to heat stress (37°C).

F. PCGs or TEs upregulated in heat-stressed WT plants were aligned at their 5'-end or 3'-end and average cytosine methylation levels in the indicated nucleotide contexts were calculated from 3 kb upstream to 3 kb downstream in a WT subjected to a control stress (23°C) or to heat stress (37°C). Upstream and downstream regions were divided in 100bp bins, while annotations were divided in 40 bins of equal length.

Figure 2

A. Heat stress-induced activation of the *L5-GUS* transgene in rosette leaves of the indicated genotypes after 24h at 23°C or 37°C detected by X-Gluc staining.

B. RT-qPCR analysis of transcripts from the *L5-GUS* transgene, normalized to the reference gene *AT5G12240* and further normalized to the mean of L5 samples at 23°C. Error bars represent standard error of the mean across three biological replicates.

C. RT-PCR analysis of transcripts from endogenous repeats. Amplification of 18S rRNAs was used as a loading control. PCR in the absence of reverse transcription (RT-) was performed to control for genomic DNA contamination.

D. Representative pictures of 16-day-old seedlings of the indicated genotypes grown in soil and in long day conditions. Scale bar: 1cm.

E. Heat survival assays. Seven-day-old seedlings of the indicated genotypes were subjected to a 37°C heat stress for 24h or 48h and returned to standard conditions for nine days. Pictures are representative of five replicates (24h 37°C) and two replicates (48h 37°C).

F. Heat stress-induced activation of the *L5-GUS* transgene in rosette leaves of the indicated genotypes after 24h at 37°C detected by X-Gluc staining.

G. Top: Gene models for *MED14* and *UVH6*, to scale. Punctual mutations (in orange) and their corresponding amino acid changes are indicated by vertical lines, their position relative to the transcriptional start site (+1) is given. Insertional transfer-DNA mutations are indicated by triangles. Location of the *med14-1* mutation is reported according to Autran et al. (2002). Bottom: Representation of MED14 and UVH6 proteins and their domains. The relative length of MED14 and UVH6 are not to scale. Point mutations and their corresponding amino acid changes are indicated by vertical lines. In MED14, LXXLL motifs have been indicated by black boxes. In UVH6, helicase motifs I, Ia, II, III, IV, V and VI are indicated by transparent white boxes, respectively from left to right. The positions of the domains were inferred from studies in other model organisms (see methods). KID : Knob Interaction Domain, RM1 and RM2 : Repeat Motif 1 and 2, TID : Tail Interaction Domain. HD1a, HD1b, HD1c, HD2 : Helicase domain 1a, 1b, 1c, 2.

Figure 3

A. Number of PCGs and TEs detected as differentially expressed in *med14-3*, *uvh6-3* and *uvh6-4* relative to the WT at 23°C.

B. Venn diagrams showing the extent of the overlap between upregulated and downregulated loci determined in *med14-3* and *uvh6-4*.

Figure 4

A. Transcriptional changes in WT plants subjected to heat stress (top), in *med14-3*_37 (middle) and *uvh6-3*_37 (bottom) relative to heat-stressed WT, represented along the chromosome five by log2 ratios of mean RPKM values in 100kb windows.

B. Number of PCGs and TEs detected as differentially expressed in *med14-3*_37 and *uvh6-3*_37 relative to the WT at 37°C.

C. Venn diagrams showing the extent of the overlap between upregulated and downregulated loci determined in *med14-3*_37 and *uvh6-3*_37

D. Log2 RPKM values in the WT at 37°C, *med14-3*_37 (left) and *uvh6-3*_37 (right) of TEs upregulated in heat-stressed WT plants.

Figure 5

A. Venn diagrams showing the upregulated TEs in *ddm1* and *mom1* and their overlap.

B. Reads per million per kilobase (RPKM) values in the indicated genotypes of transposable elements (TEs) commonly upregulated between *ddm1* and *mom1*. Progenies from sister plants were identically colored. Statistical differences between distributions of single mutants (*ddm1* and *mom1*) versus double mutants (*med14 ddm1*, *uvh6 ddm1*, *med14 mom1*, *uvh6 mom1*) were tested by unpaired two-sided Mann-Whitney test.

C. Transcripts from *TSI* and *MULE* loci were analyzed by RT-qPCR in rosette leaves from indicated genotypes at control temperature (23°C). Data were normalized to the reference gene *AT5G12240* and further normalized to the mean of L5 samples at 23°C. Error bars illustrate standard errors of the mean across three biological replicates. Statistically significant differences between means of *mom1*, *ddm1*, *met1* and combinations of these mutations with *med14-3* were tested by unpaired bilateral Student's t-test.

D. DNA methylation levels at CG, CHG and CHH contexts of TEs upregulated in heat-stressed WT samples, distinguishing TEs downregulated in *med14-3* from TEs not downregulated in *med14-3*, were calculated in WT samples subjected to a control stress at 23°C. Statistical differences between data sets were tested by unpaired two-sided Mann-Whitney test.

E. RPKM values at TEs were calculated using multi- and uniquely-mapped reads in WT and *med14-3* in control conditions (23°C) (see methods). TEs above one RPKM in WT were grouped according to their log2 fold change in *med14-3* and DNA methylation levels at CG, CHG and CHH contexts in WT at 23°C were calculated for each group. Statistical differences between data sets were tested by unpaired two-sided Mann-Whitney test.

Figure 6

A. Kernel density plot of DNA methylation differences between *med14-3* and WT at CG, CHG and CHH contexts.

B. Number of 100-bp differentially methylated regions (DMRs) detected in *med14-3* at CG, CHG and CHH contexts with a minimum DNA methylation difference of 0.4, 0.2 and 0.2, respectively.

C. Chromosomal density of hypo-CHG (blue) and hypo-CHH DMRs (red) identified in *med14-3* (top) with total TE density in grey (bottom), both calculated by 100 kb windows on chromosome 3.

D. DNA methylation levels in CHH context in the indicated genotypes at *med14-3* hypo-CHH DMRs.

E. DNA methylation levels in CHH context in the indicated genotypes at 1200 randomly selected regions of 100 bp.

Supplementary figure 1

Transcript accumulation in rosette leaves from Col-0 wild type (WT), *arp6-1* and *atmorc6-3* mutants was quantified by RT-qPCR at five loci overexpressed in heat-stress. Samples had been subjected to a control stress at 23°C or a heat stress treatment at 37°C. Data were normalized to the geometric mean of the reference genes *AT5G12240* and *ACT2*. Values were further normalized to the mean of L5 samples at 23°C. Error bars indicate standard errors of the mean across three biological replicates. For each locus, differences in mean at 37°C between the WT and the mutants was tested by unpaired two-tailed Student's t-test, but did not reveal any significant difference ($P > 0.05$).

Supplementary figure 2

A. PCGs or TEs were aligned at their 5'-end or 3'-end and average cytosine methylation levels in the indicated nucleotide contexts were calculated from 3 kb upstream to 3 kb downstream in WT subjected to a control stress (23°C) or to heat stress (37°C). Upstream and downstream regions were divided in 100bp bins, while annotations were divided in 40 bins of equal length.

B. Average cytosine methylation levels at PCGs or TEs upregulated or downregulated in heat-stressed WT plants were calculated and represented as in A.

Supplementary figure 3

A. X-Gluc staining of heat-stressed rosette leaves from a complementation tests between *zen1* and *zen2* mutants.

B, C. Segregants with a suppressor phenotype in a F2 population from a mutant (Col-0) x Ler-0 cross were sequenced in bulk. Y axis indicates SNP frequencies along 20kb windows. The SNP-depleted chromosomal region encompasses homozygous candidate mutations, as indicated by an orange rectangle. B. *zen1* mapping C. *zen2* mapping

Supplementary figure 4

Protein sequence alignment of XPD orthologs from *Saccharomyces cerevisiae* (Sc_RAD3), *Homo sapiens* (Hs_XPD) and *Arabidopsis thaliana* UVH6 (At_UVH6). The alignment was performed with Clustal Omega (v1.2.4). UVH6 point mutations and their corresponding amino acid changes are indicated.

Supplementary figure 5

A. Heat stress-induced activation of the *L5-GUS* transgene in rosette leaves of the indicated genotypes after 24h at 37°C was detected by X-Gluc staining.

B. RT-qPCR analysis of transcripts from *L5-GUS* and *MULE*, normalized to the reference gene *AT5G12240* and further normalized to the mean of L5 samples at 23°C. Errors bars represent standard error of the mean across two biological replicates. Statistically significant differences between means of *uvh6-3* and *uvh6-4* samples at 37°C were tested by unpaired unilateral Student's t-test (*: p-value < 0.05, **: p-value < 0.005).

C. Representative pictures of 16-day-old seedlings of the indicated genotypes grown in soil and in long day conditions. Scale bar: 1cm.

Supplementary figure 6

A. Reads per million per kilobase (RPKM) values in the WT and *uvh6-3* mutants of loci significantly upregulated and downregulated in *uvh6-4* at 23°C. Statistical differences between distributions in WT and *uvh6-3* were tested by unpaired two-sided Mann-Whitney test.

B. UV survival assays. Seven-day-old seedlings of the indicated genotypes were UV irradiated at 10kJ / m2, returned to standard conditions with 24h of dark followed by five days recovery in light.

Supplementary figure 7

Transcriptional changes in WT plants subjected to heat stress (top), in *med14-3*_37 (middle) and *uvh6-3*_37 (bottom) relative to heat-stressed WT, represented along chromosomes one to four by log2 ratios of mean RPKM values in 100kb windows.

Supplementary figure 8

A. Log2 RPKM values in the WT at 37°C, *med14-3*_37 (left) and *uvh6-3*_37 (right) of PCGs upregulated in heat-stressed WT plants.

B. Log2 RPKM values in the WT at 37°C, *med14-3*_37 (left) and *uvh6-3*_37 (right) of PCGs downregulated in heat-stressed WT plants.

C. RPKM log2 fold change (log2FC) of loci (PCGs and TEs) differentially expressed in *med14-3*_37 (left) and *uvh6-3*_37 (right) showed for both *med14-3*_37 and *uvh6-3*_37 relative to heat-stressed WT plants.

D. Relative frequency of TE superfamilies in the Arabidopsis genome (TAIR10, white) and the following datasets: TEs upregulated in WT plants subjected to heat stress (red), among these, TEs downregulated in *med14-3*_37 (dark blue) or in *uvh6-3*_37 (green) relative to a WT at 37°C.

Supplementary figure 9

Transcripts from six loci were analyzed by RT-qPCR in L5 control plants, *med14-3*, *uvh6-3* mutants and *med14-3 uvh6-3* double mutants at 23°C and 37°C. Data were normalized to the reference gene *AT5G12240* and further normalized to the mean of L5 samples at 23°C. Error bars illustrate standard errors of the mean across three biological replicates. For each temperature treatment, statistical differences between means of mutant conditions were tested by ANOVA followed by post-hoc analysis using Tukey's Honest Significant Difference test (*: p-value < 0.05, **: p-value < 0.005, ***: p-value < 0.0001). See methods. Data for the *L5-GUS* transgene was already displayed in figure 2B.

Supplementary figure 10

A, B. Reads per million per kilobase (RPKM) values in the indicated genotypes of transposable elements (TEs) upregulated in *ddm1* (A) or *mom1* (B). Sister plants were identically colored. Statistical

differences between distributions of single mutants (*ddm1* and *mom1*) versus double mutants (*med14 ddm1*, *uvh6 ddm1*, *med14 mom1*, *uvh6 mom1*) were tested by unpaired two-sided Mann-Whitney test.

C. TEs commonly upregulated in *ddm1* and *mom1* were aligned at their 5'-end or 3'-end and average cytosine methylation levels in the indicated nucleotide contexts were calculated from 3 kb upstream to 3 kb downstream in WT, *ddm1* and *mom1*. Upstream and downstream regions were divided in 100bp bins, while annotations were divided in 40 bins of equal length.

D. DNA methylation levels at CG, CHG and CHH contexts were calculated for TEs upregulated in heat-stressed WT samples, distinguishing TEs downregulated in *med14-3* from TEs not downregulated in *med14-3*. DNA methylation levels were calculated in WT at 23°C and 37°C.

E. DNA methylation levels at CG, CHG and CHH contexts were calculated for TEs upregulated in heat-stressed WT samples, distinguishing TEs downregulated in *uvh6-3* from TEs not downregulated in *uvh6-3*. DNA methylation levels were calculated in WT at 23°C and 37°C.

Supplementary figure 11

A. TEs localized in chromosome arms or pericentromeres were aligned at their 5'-end or 3'-end and average cytosine methylation levels in the indicated nucleotide contexts were calculated from 3 kb upstream to 3 kb downstream in WT and *med14-3*. Upstream and downstream regions were divided in 100bp bins, while annotations were divided in 40 bins of equal length.

B. Average DNA methylation levels were calculated at protein coding genes as in A.

C. DNA methylation levels in CG, CHG and CHH contexts in WT and *med14-3* at *med14-3* hypo-CHG DMRs (left) and *med14-3* hypo-CHH DMRs (right).

Supplementary figure 12

A. DNA methylation levels in CHG context in WT and *nrpb2-3* at *med14-3* hypo-CHG DMRs (left). DNA methylation in CHH context in WT and *nrpb2-3* at *med14-3* hypo-CHH DMRs (right). Two replicates are shown for each genotype.

B. DNA methylation levels in CHG context in the indicated genotypes at *med14-3* hypo-CHG DMRs.

C. DNA methylation levels in CHH context in WT and *med14-3* at hypo-CHH DMRs identified in *drm1/2*, *nrpd1* and *nrpe1*. Statistically significant differences between distributions in WT and *med14-3* were tested by unpaired two-sided Mann-Whitney test.

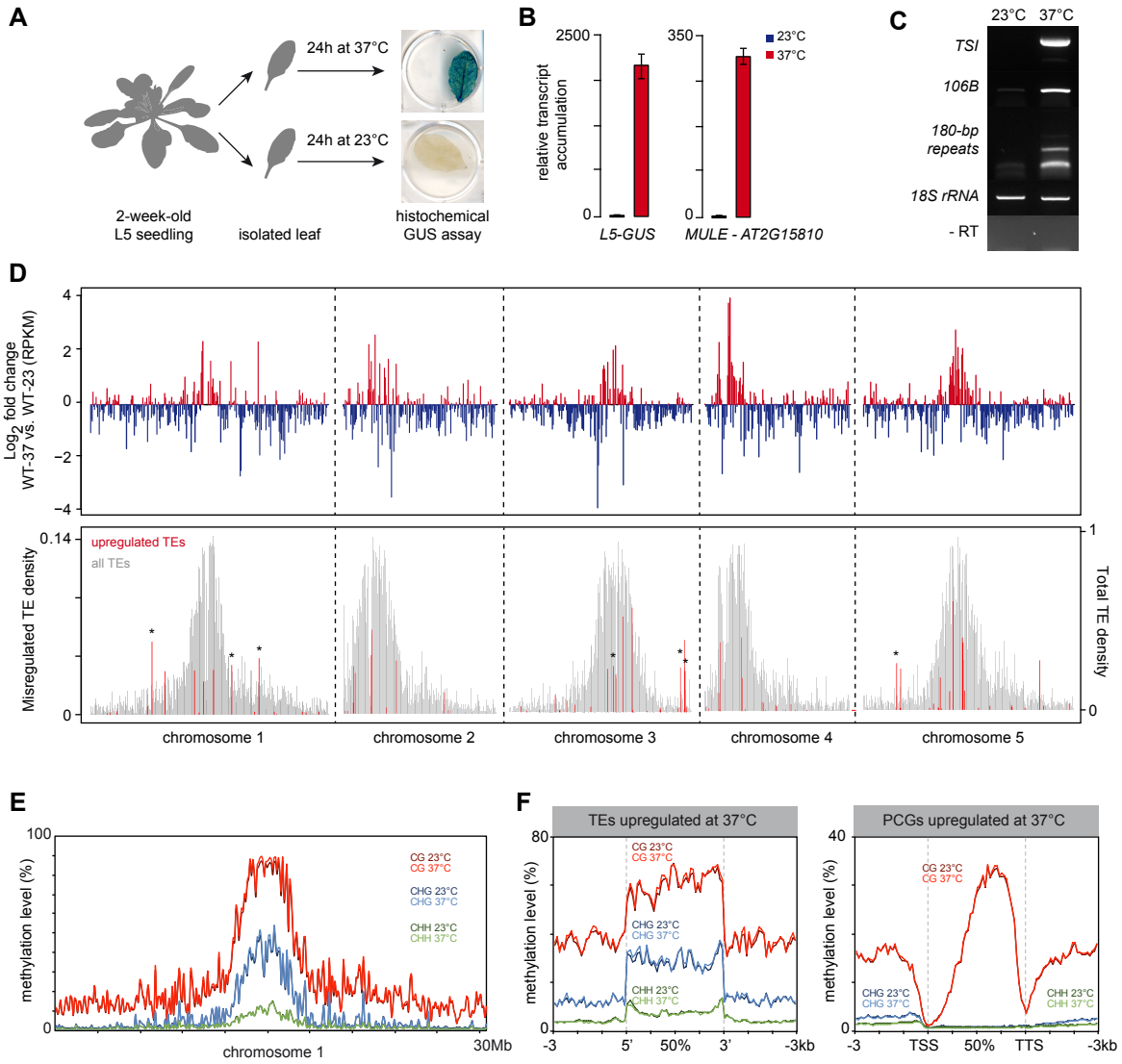

Figure 1

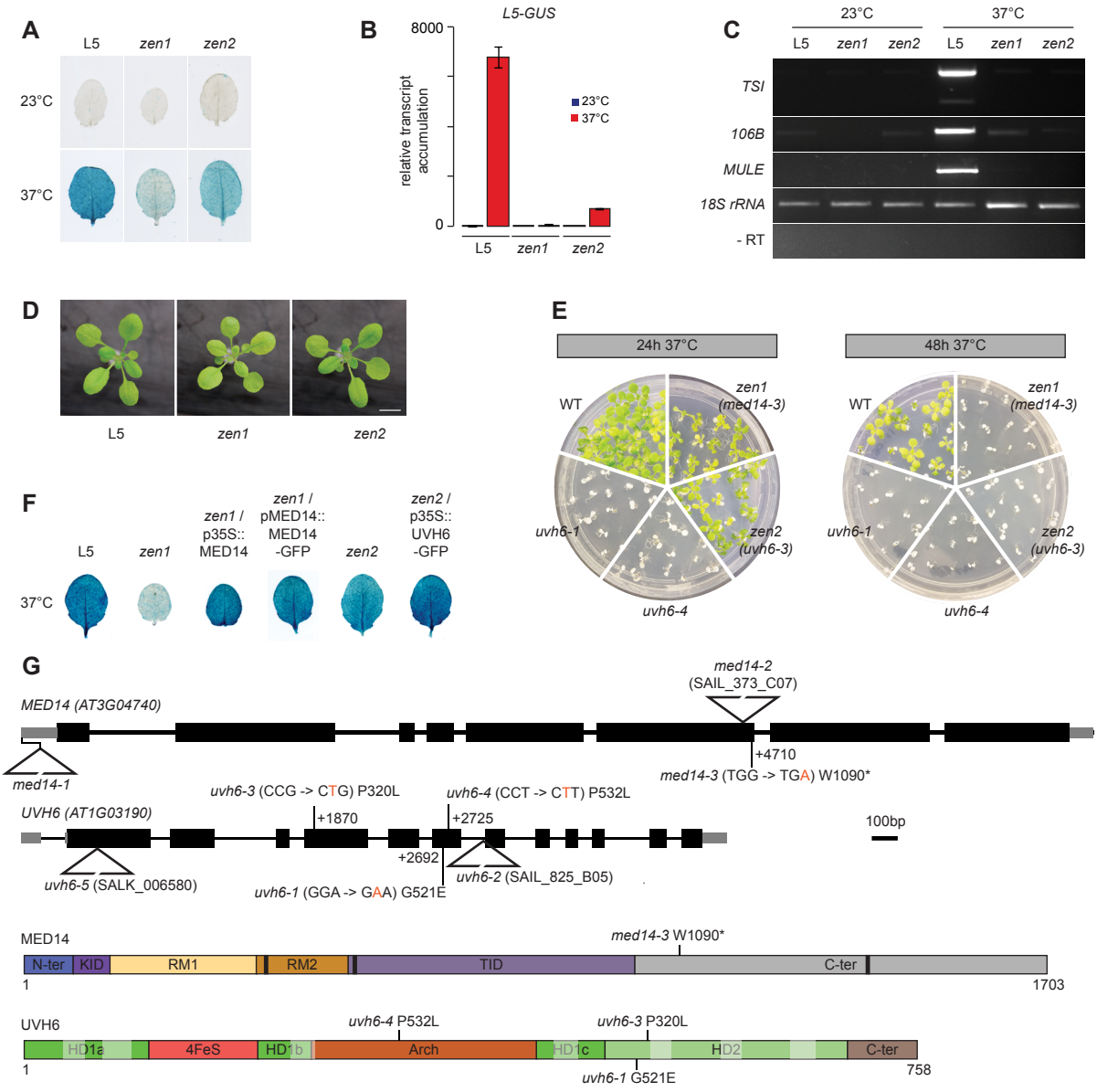

Figure 2

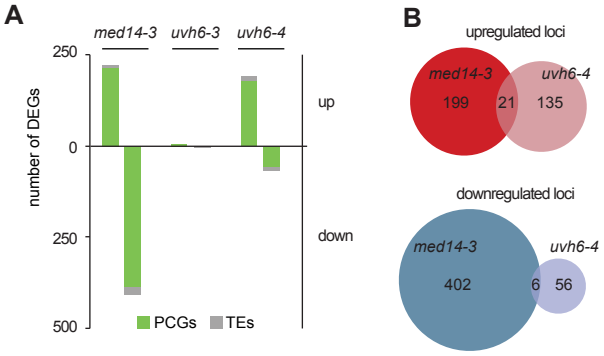

Figure 3

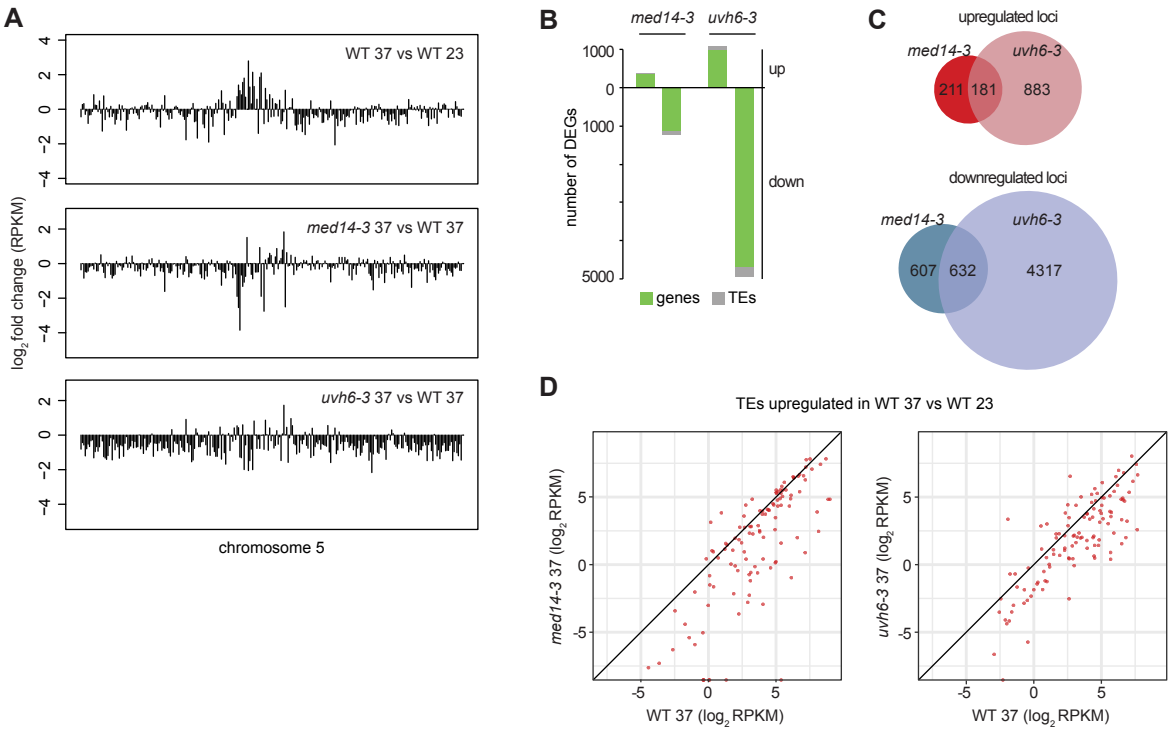

Figure 4

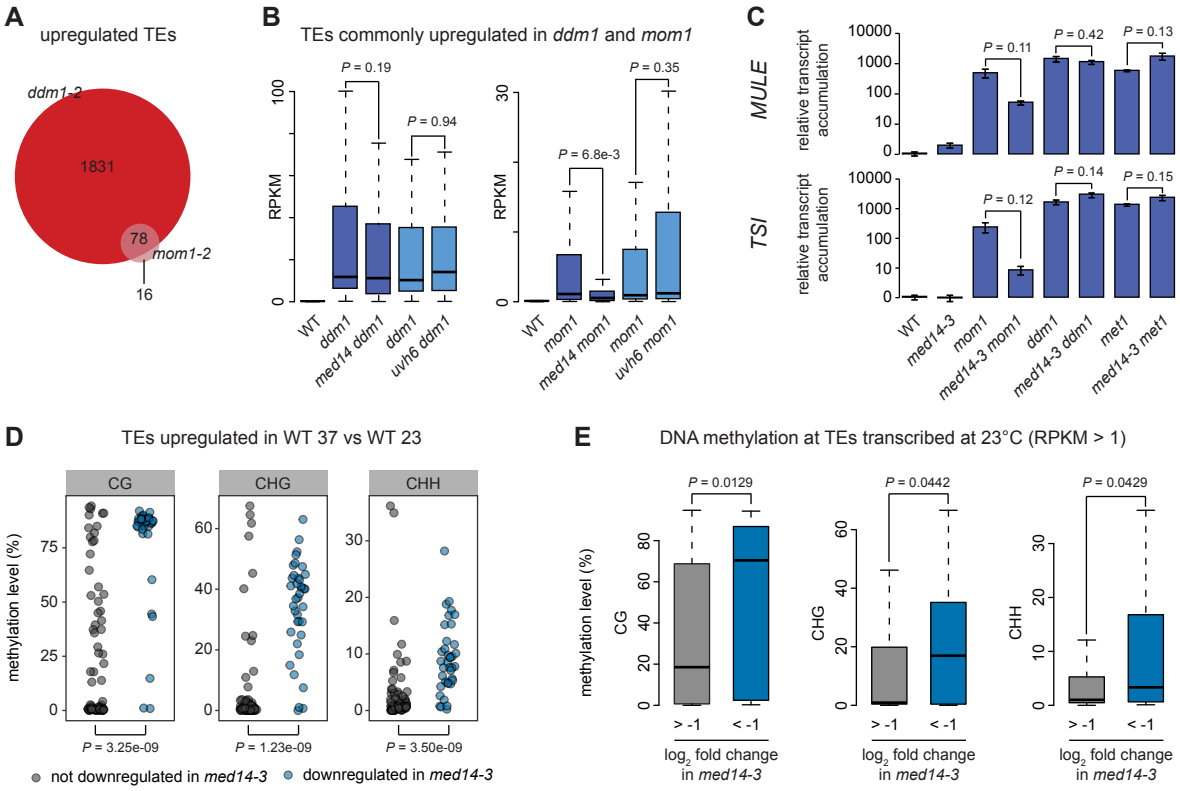

Figure 5

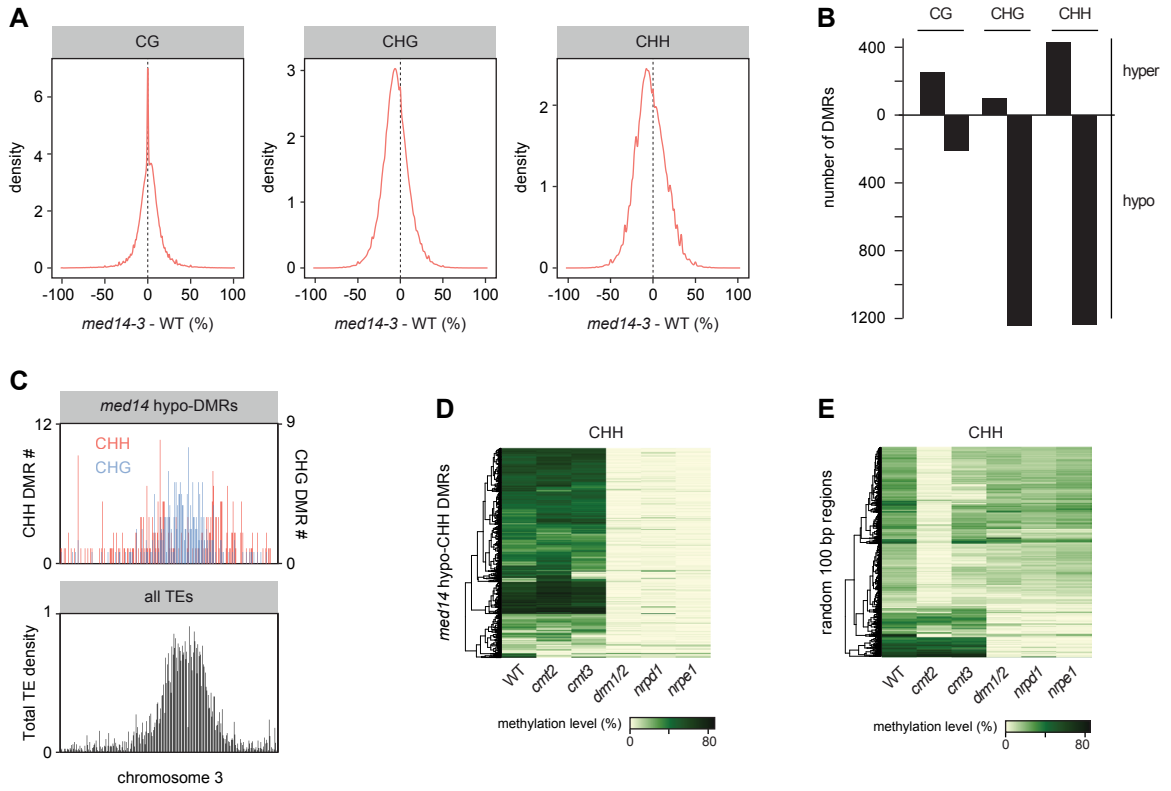

Figure 6